Received: 21 November 2025 | Revised: 17 February 2026 | Accepted: 27 February 2026

DOI: 10.1002/pro.70536

RESEARCH ARTICLE

THE PROTEIN SOCIETY WILEY

Understanding cell-penetrating peptide mechanisms using computational electrophysiology simulations

Eric Catalina-Hernandez[1,2] | **Marcel Aguilella-Arzo**[3] | **Mario Lopez-Martin**[1,2] | **Alex Peralvarez-Marin**[1,2]

[1]Unit of Biophysics, Department of Biochemistry and Molecular Biology, Facultat de Medicina, Universitat Autònoma de Barcelona, Cerdanyola del Vallès, Catalonia, Spain

[2]Institute of Neurosciences, Universitat Autònoma de Barcelona, Cerdanyola del Vallès, Catalonia, Spain

[3]Laboratory of Molecular Biophysics, Department of Physics, University Jaume I, Castellon, Spain

Correspondence
Alex Peralvarez-Marin and Eric Catalina-Hernandez, Department of Biochemistry and Molecular Biology, Unit of Biophysics, Facultat de Medicina, Universitat Autònoma de Barcelona, Av. Can Domènech s/n, 08193 Cerdanyola del Vallès, Catalonia, Spain.
Email: alex.peralvarez@uab.cat and ericatalinah@gmail.com

Funding information
Universitat Jaume I, Grant/Award Number: UJI-B2022-42; Ministerio de Ciencia Innovacion y Universidades, Grant/Award Numbers: Margarita Salas Award-MGSD2021-10, MCIN/AEI/49010.13039/501100011033, PID2020-120222GB-489I00, PID2022-142795NB-I00; Universitat Autònoma de Barcelona, Grant/Award Number: B21P0033

Review Editor: Lynn Kamerlin

Abstract

Cell-penetrating peptides (CPPs) can enter cells without inducing cytotoxicity and can be coupled with cargo molecules to be used to deliver drugs, DNA, or nanoparticles into cells. The peptide-membrane interactions driving the internalization mechanism are not completely understood. In this study, we introduce Computational Electrophysiology (CompEL) as a tool for the computational investigation of CPP and membrane interaction leading to internalization, focusing on cationic CPPs such as Arg9, MAP, TP10, and TP2. CompEL induces membrane stress through ion imbalance, prompting the membrane to alleviate this stress via pore formation. Using double bilayer molecular dynamics (MD) simulations with one or eight peptides, we show that CPPs can use these pores to translocate, whereas non-CPP non-aleucine peptide fails to cross the membrane and instead contributes to pore stabilization. In the eight-peptide systems we observe that some peptides can cooperate to reach translocation or to foster pore stabilization. This study introduces CompEL as a powerful tool for CPP research, shedding light into the molecular peptide-membrane interactions governing CPP translocation, and offering valuable insights for the design of next-generation delivery systems.

KEYWORDS
cell-penetrating peptides, computational electrophysiology, molecular dynamics, peptide cooperativity, pore dynamics

1 | INTRODUCTION

Cell-penetrating peptides (CPPs) represent a diverse class of molecules renowned for their ability to traverse biological membranes and facilitate the intracellular delivery of various cargoes without inducing cytotoxicity (Bertrand et al., 2009; Copolovici et al., 2014; Lindgren et al., 2000). CPPs can internalize into cells coupled with various cargoes, such as proteins, DNA, RNA, nanoparticles or low molecular weight drugs (Endoh & Ohtsuki, 2009; Kristensen et al., 2016; Li et al., 2012; Säälik et al., 2004; Silva et al., 2019; Veldhoen et al., 2006). Moreover, CPPs are currently being used for therapeutic purposes, such as cancer treatment, Alzheimer's disease, and immunotherapy (Fathi et al., 2025; Klimpel et al., 2019; Lee et al., 2025;

Magzoub, 2020; Wu et al., 2019). Nevertheless, the molecular mechanism of CPP translocation and internalization requires further investigation (Muñoz-Gacitúa et al., 2022), for controlled rational design of these biomedically relevant molecules.

Many molecular mechanisms have been proposed, which can be classified into energy-dependent and energy-independent methods (Catalina-Hernandez & Peralvarez-Marin, 2026; Gestin et al., 2017). Energetic mechanisms entail endocytosis and vesicle formation (Richard et al., 2005; Ruseska & Zimmer, 2020; Thorén et al., 2003), whereas energy-independent mechanisms include pore formation (Matsuzaki et al., 1996), which can happen through the toroidal (involving lipids in the pore stabilization process) (Bechara & Sagan, 2013) or the barrel-stave (without the use of lipids to stabilize the pore) (Copolovici et al., 2014) models, the carpet model (through membrane destabilization) (Pouny et al., 1992), the membrane thinning model (Lee et al., 2005), and inverted micelle (Derossi et al., 1996). More recently, CPPs have been discovered to translocate across both the endosomal and plasma membranes by a vesicle budding and collapse (VBC) mechanism (Sahni et al., 2020, 2024). In fact, the diverse possible translocation methods lead to talk about a *landscape* of different internalization mechanisms (Langel, 2019). In addition to these mechanisms, other variables, such as peptide concentration, can also affect the internalization dynamics (Magzoub et al., 2002).

CPPs exhibit a wide range of structural and biochemical characteristics, often classified based on their predominant physicochemical properties. Among these classifications, peptides can be categorized as cationic, hydrophobic, amphipathic or stimuli-responsive (Hunt et al., 1997; Milletti, 2012). Cationic peptides, such as Arg9 (Futaki et al., 2001) are characterized by an abundance of positively charged residues, such as arginine or lysine, which promote electrostatic interactions with negatively charged cell membranes. Hydrophobic peptides, such as TP2 (Marks et al., 2011), and K-FGF (Lin et al., 1995) possess a high proportion of hydrophobic residues, facilitating interactions with lipid bilayers. Amphipathic peptides, such as TP10 (Soomets et al., 2000) or MAP (Lindgren et al., 2000; Steiner et al., 1991), can be further divided into primary amphipathic (featuring distinct hydrophobic and hydrophilic regions within their sequences), secondary amphipathic (which adopt amphipathic conformations upon interaction with lipid membranes), proline-rich, and histidine-rich (Iwasaki et al., 2015; Milletti, 2012). Stimuli-responsive CPPs, such as pH-(low)-insertion-peptide (An et al., 2010; Hunt et al., 1997) and the histidine-rich synthetic peptide LAH4-L1 (Wolf et al., 2017) exhibit their activity under certain conditions, for instance, under acidic pH. Understanding the classification of CPPs based on these physicochemical properties is essential for elucidating their mechanisms of cell penetration and optimizing their utility in biomedical applications (De Oliveira et al., 2022).

Molecular dynamics (MD) simulations have been extensively used to investigate the internalization mechanisms, since they can provide meaningful insights of peptide-membrane interaction at atomic level (Catalina-Hernandez & Peralvarez-Marin, 2026; Magzoub et al., 2001, 2005; Thorén et al., 2004). In this study, we seek to study the insertion or translocation abilities of CPPs. Nonetheless, the translocation process takes from seconds to minutes (Kutzner et al., 2011; Yesylevskyy et al., 2009), and is too computationally demanding to be observed in a conventional Molecular Dynamics (cMD) simulation. In this regard, enhanced sampling techniques have been employed to explore a larger conformational space, such as Umbrella Sampling (US) (Huang & García, 2013; Torrie & Valleau, 1977), Replica Exchange (RE) (Nymeyer et al., 2005; Reid et al., 2019), adaptive Steered Molecular Dynamics (aSMD) in combination with cMD (Catalina-Hernandez, Aguilella-Arzo, et al., 2025), and Weighted Ensemble (WE) (Choe, 2021). Besides, coarse graining techniques, such as MARTINI, have also been used to study the thermodynamics of CPP translocation (Hu et al., 2014) (interested readers are redirected to the exhaustive review by Ouyang and colleagues; Ouyang et al., 2022). However, these methods have inherent limitations. For instance, US is primarily used to calculate the free energy of translocation, aSMD requires powerful computational resources, and they are strongly biased methods requiring reaction coordinates, whereas coarse-grained simulation have lower resolution. Therefore, we repurpose computational electrophysiology (CompEL) (Kutzner et al., 2011) to elucidate the key steps involved in CPP cell penetration. CompEL has been previously used to study membrane proteins, mainly ion channels (see the CompEL review in (Kutzner et al., 2016)), but, to the best of our knowledge, this is the first study to employ CompEL for the study of CPPs and their mechanism of action.

Simulations at high temperatures (up to 500 K) have been performed to study membrane disruption of small molecules (Wang et al., 2019), following the high kinetics rationale to enhance sampling (Daggett & Levitt, 1992). Following a parallel reasoning, in CompEL, we generate a difference in potential through ion imbalance using a double membrane configuration (Kutzner et al., 2011), allowing for enhanced sampling and easier CPP-mediated membrane disruption. Through this approach, we seek to identify critical molecular events and kinetic barriers that dictate the efficiency of CPP internalization. We aim to provide a new possibility to unravel the interactions between

CPPs and lipid membranes, shedding light on the processes governing their cellular uptake.

In this regard, we chose four representative CPPs (Arg9, MAP, TP10, and TP2) to compare them with our previous study (Catalina-Hernandez, Aguilella-Arzo, et al., 2025) and a negative control (Leu9, non-CPP) to conduct the study. First, we ran simulations with one peptide at different potentials to decide the appropriate transmembrane potential for this system setup. Then, we analyzed the simulations at the chosen transmembrane potential. Last, we simulated the systems with eight peptides to study and analyze CPP cooperation and aggregation.

In this study, we aim to expand the computational toolkit for investigating membrane-active peptides (Avci et al., 2018; Sani & Separovic, 2016), with a particular emphasis on CPPs. To this end, we employ CompEL, an entry-level, rapid, and reproducible computational technique, to explore the molecular mechanisms underlying CPP internalization. Our objectives are to differentiate between CPP-like and non-CPP peptides and to compare single- to multiple-peptide simulations. Our findings hold promise for guiding the rational design of CPP-based delivery systems and advancing targeted therapeutic interventions in biomedical research.

2 | MATERIALS AND METHODS

2.1 | Systems preparation

Peptides were initially modeled with ColabFold notebook (Mirdita et al., 2022), which uses AlphaFold (Jumper et al., 2021) monomer prediction to model the peptides. Each peptide was put in a 7.5 × 7.5 × 7.5 nm box solvated with TIP3 waters. The systems were minimized for 5000 steps, equilibrated in the NVT ensemble for 125,000 steps, and the production was run for 250 ns. The forcefield chosen was CHARMM36m, which has been maintained throughout the study. GROMACS (Abraham et al., 2015; Bekker et al., 1993; Berendsen et al., 1995; Hess et al., 2008; Lindahl et al., 2001; Páll et al., 2015; Pronk et al., 2013; Van Der Spoel et al., 2005) software was used to run the simulations. The temperature of all the simulations was maintained at 350 K, to use the same temperature that is going to be used in CompEL. Periodic boundary conditions (PBC) were applied.

The simulations were analyzed using Jupyter Notebook integrated development environment (IDE) (Kluyver et al., 2016) and GROMACS. The trajectory of the peptide was clustered using the MDAnalysis package in Python (Gowers et al., 2016; Michaud-Agrawal et al., 2011), and the centroid structure was used as input for the CompEL simulations run using GROMACS.

The membrane was composed of 128 POPC (1--palmitoyl-2-oleoylphosphatidylcholine) molecules per leaflet (256 POPC each bilayer and 512 in total in the system) and solvated with TIP3P water. The system was neutralized with KCl to a final concentration of 150 mM. The systems were built using CHARMM-GUI (Jo et al., 2008; Lee et al., 2016; Wu et al., 2014) web server. The system box size was 9.35 × 9.35 × 17 nm.

2.2 | CompEL simulations

In CompEL, a transmembrane potential triggered by charge imbalance (ΔQ) between the two aqueous compartments separated by the membrane is used to generate an electric potential difference across a lipid bilayer. In this approach, the electrostatic potential arises self-consistently from the excess ions, rather than from an externally applied electric field. Since PBC are applied in all three spatial dimensions, a single membrane system would not sustain a stable transmembrane potential, as the aqueous compartments on either side of the bilayer are periodically connected. To overcome this limitation, a double membrane configuration was designed, creating two independent water compartments separated by two membranes. This setup allows a well-defined and stable charge imbalance to be maintained between the inner and outer aqueous regions, resulting in a constant transmembrane potential across each bilayer.

The double membrane system was prepared following established CompEL protocols (Kutzner et al., 2011, 2016; Weng et al., 2021). First, the equilibrated single-bilayer system was duplicated, the second copy was rotated, the simulation box size was doubled along the membrane normal, and both systems were concatenated into a single simulation box. GROMACS built-in *gmx* utilities were used. The desired charge imbalance was then introduced by adding positive charges (K^+ ions) in the inner water compartment and negative charges (Cl^- ions) in the outer water compartment, while maintaining overall electro neutrality of the simulation box. Ion insertion was performed by swapping water molecules with ions using the GROMACS utility *gmx insert-molecules*. In Table 1, we present the configurations for all the systems simulated in this study, indicating the resulting charge imbalances, corresponding membrane potentials, and ionic conditions. Based on the compartment volume of approximately 350 nm^3, the effective KCl concentration was determined by the number of stoichiometric ion pairs (K^+/Cl^-). While the number of pairs varies with ΔQ, the total number of mobile ions in each compartment was maintained at 56. Thus, the ionic strength remained constant at approximately 133 mM across all simulations. The ion number was kept constant in each water compartment through the whole duration of the simulation using the computational electrophysiology protocol in GROMACS, which controls ion/water position

TABLE 1 System configurations in the computational electrophysiology (CompEL) method.

Transmembrane potential (ΔQ)	# K+ in OWC	# K+ in IWC	# Cl- in OWC	# Cl- in IWC	# water residues	Effective [KCl] (mM)	Ionic strength (mM)
0	28	28	28	28	22,850	133	133
8	30	26	26	30	22,820	123	133
12	31	25	25	31	22,831	119	133
16	32	24	24	32	22,839	114	133
24	34	22	22	34	22,832	104	133

Note: The composition is indicated for the system without peptides (membrane only, control simulations). When a peptide is added to the system (in the outer water compartment), the corresponding counterions were added (in the same water compartment). OWC and IWC refer to the outer and the inner water compartments, respectively.

TABLE 2 Summary of the simulations and replicas run in this study.

Number of peptides	0 ΔQ	8 ΔQ	12 ΔQ	16 ΔQ	24 ΔQ
1	3 replicas	3 replicas	3 replicas	3 replicas	3 replicas
8	3 replicas	3 replicas	3 replicas	3 replicas (500 ns)	–

Note: The columns show the different transmembrane potential through ion imbalance (ΔQ) used, and the rows indicate the number of peptides. If not indicated otherwise, the simulations have been run for 250 ns.

exchanges (production files can be found at the GitHub repository, see Section 2.4). In simulations containing a peptide, the peptide was added in the inner water compartment, along with the corresponding counterions, following the same procedure as before. Thereafter, the system was minimized for 5000 steps and equilibrated for approximately 2 ns (the different steps were of 125, 125, 125, 500, 500, and 500 ps) while gradually lowering the positional restraints (1000, 400, 400, 200, 40, and 0 $kJ \cdot mol^{-1} \cdot nm^{-2}$, respectively). Last, a 250 ns simulation was run for each system, with three replicas in each case. All simulations were run at 350 K to allow more mobility (Maragliano & Vanden-Eijnden, 2006). Lipids and peptides were described using the CHARMM36m force field. Long-range electrostatic interactions were treated using the particle mesh Ewald (PME) method with a real-space cutoff of 1.2 nm, while van der Waals interactions were force-switched between 1.0 and 1.2 nm using a Verlet cutoff scheme. A summary of the number of simulations run can be found at Table 2, accounting for approximately 42 μs of simulation time (ca. 4 μs for membrane only systems, ca. 19 μs for systems with one peptide, and 19 μs for systems with eight peptides). The simulations were run using a workstation with a GPU RTX3080Ti, at approximately 80 ns per day.

2.3 | Data analysis

MD simulation analysis was executed in a Jupyter Notebook IDE (Kluyver et al., 2016), used along with the MDAnalysis package in Python, and *gmx* utilities (Gowers et al., 2016; Hess et al., 2008; Lindahl et al., 2001; Michaud-Agrawal et al., 2011; Pronk et al., 2013; Van Der Spoel et al., 2005). PyLipID was used to analyze lipid occupancy, which is a measure of the simulation time that a protein residue is in contact with the lipids (Song et al., 2022). Visual inspection and molecular graphics were performed in VMD (Humphrey et al., 1996). Secondary structure was analyzed in VMD, which uses the STRIDE program (Frishman & Argos, 1995) as the built-in secondary structure algorithm.

The transmembrane potential corresponding to each imposed charge imbalance (ΔQ) was estimated from electrostatic potential profiles calculated using the GROMACS tool *gmx potential*. The electrostatic potential was obtained by averaging the charge density along the membrane normal (z-axis). To obtain a well-defined reference potential, this analysis was performed over the initial 10 ns of the simulations, during which the membrane structure and ion distributions remained stable. The electric field was obtained by computing the slope at each point of the potential plot.

Pore radius was calculated using an in-house Python implemented with the Scipy library (Virtanen et al., 2020). For each simulation frame, the pore region was divided along the z direction into consecutive slabs (z-stacks) of 2 Å thickness. Within each z-stack, the positions of water oxygen atoms were extracted, and pairwise Euclidian distances between all water molecules in that slab were calculated. The maximum distance between any two water molecules within a given z-stack was used to calculate the local pore radius at that axial position. This procedure was repeated for all z-stacks along the pore axis, and the minimum radius among all z-stacks was taken as the pore radius for that simulation frame, representing the narrowest constriction of the pore. The analysis was performed independently for each frame of the trajectory.

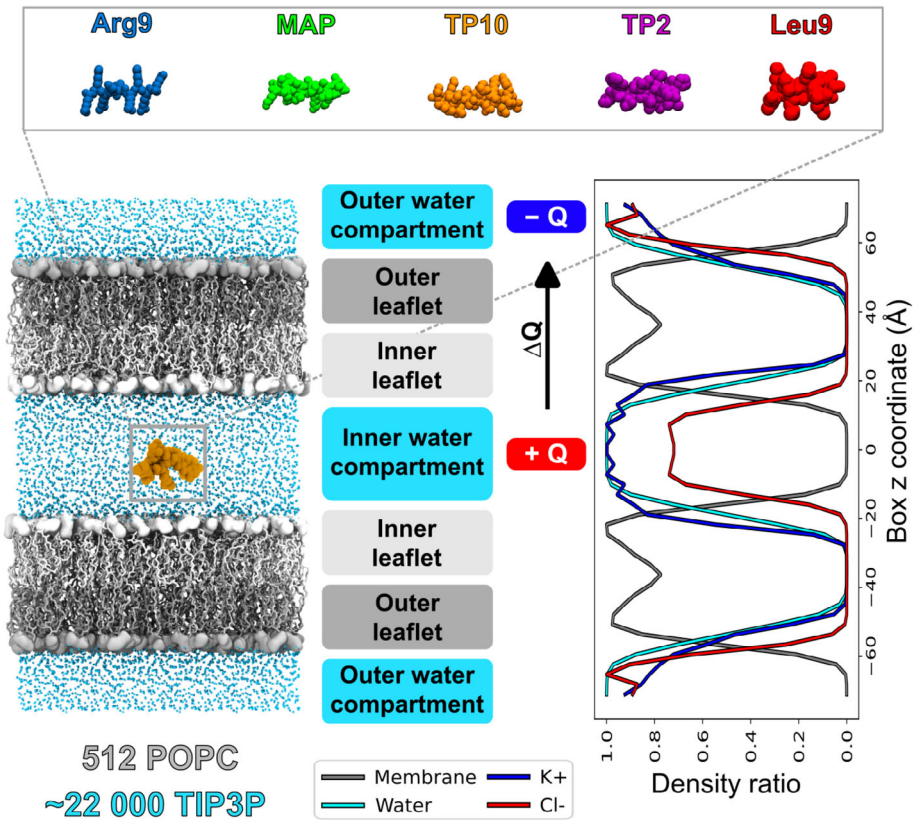

FIGURE 1 Graphical representation of CompEL initial configuration. (Top part) Modeled structure of Arg9, MAP, TP10, TP2 and Leu9 peptides. Peptides are represented as Van der Waals spheres, and colored as: Arg9 in cornflower blue, MAP in green, TP10 in orange, TP2 in purple, Leu9 in red. (Left part) The initial configuration of the membrane is shown, specifying the total number of lipid molecules, in both bilayers, and water molecules. The gray box and the peptide colored in orange indicate the starting position of the peptide in the CompEL simulation. The polar heads (phosphate and choline groups) of the phospholipids are represented as surface, and the lipid tails are represented as licorice. The inner and outer leaflets are colored in light and dark gray, respectively. Waters are represented as licorice and colored in cyan. Hydrogens are hidden for clarity. In addition, we name the different compartments in the system, differentiating between the inner and outer water compartments, and the inner and outer leaflets. The desired transmembrane potential through ion imbalance (ΔQ) is achieved by adding the same number of positive (K^+) and negative (Cl^-) charges in the inner and outer water compartments, respectively. This ΔQ is represented by the arrow and the red and blue boxes in the figure. (Right part) The electron density ratio plot of the system is shown, differentiating between membrane part, water molecules, and K^+ and Cl^- ions.

Lipid order parameter of C-H bonds (S_{CH}) computes the orientation of the lipids with respect to the membrane normal (Repáková et al., 2005). S_{CH} is calculated using Equation 1:

$$S_{CH} = \left\langle \frac{3 \cdot \left(\cos^2 \theta_{CH}\right) - 1}{2} \right\rangle \quad (1)$$

where θ stands for the angle between the C-H bond of an acyl chain and a reference axis (the z axis in MD simulations), and the angular brackets indicate an ensemble average over time and lipid molecules. S_{CH} has negative values in lipid membranes, and thus it is usually reported as $-S_{CH}$ (Piggot et al., 2017). S_{CH} has been computed for the palmitoyl (at position sn-1) chain of POPC. All analysis scripts are available at our GitHub repository (see Section 2.4). Matplotlib (Hunter, 2007) was used for plotting Figures 1–5.

2.4 | Data availability

The data supporting this article have been included as part of the Supplementary Information. System, file simulation inputs, and code to reproduce the analyses presented can be found at:

https://github.com/APMlab-memb/CompEL_CPPs.git. Due to file size limitations, the simulation trajectory file will be shared upon request.

3 | RESULTS & DISCUSSION

3.1 | ΔQ benchmarking

In order to conduct the CompEL simulations, we created a series of systems with increasing ΔQ, starting from 0 (0 net charge in any of the two compartments) to 24, where the charge imbalance was obtained by

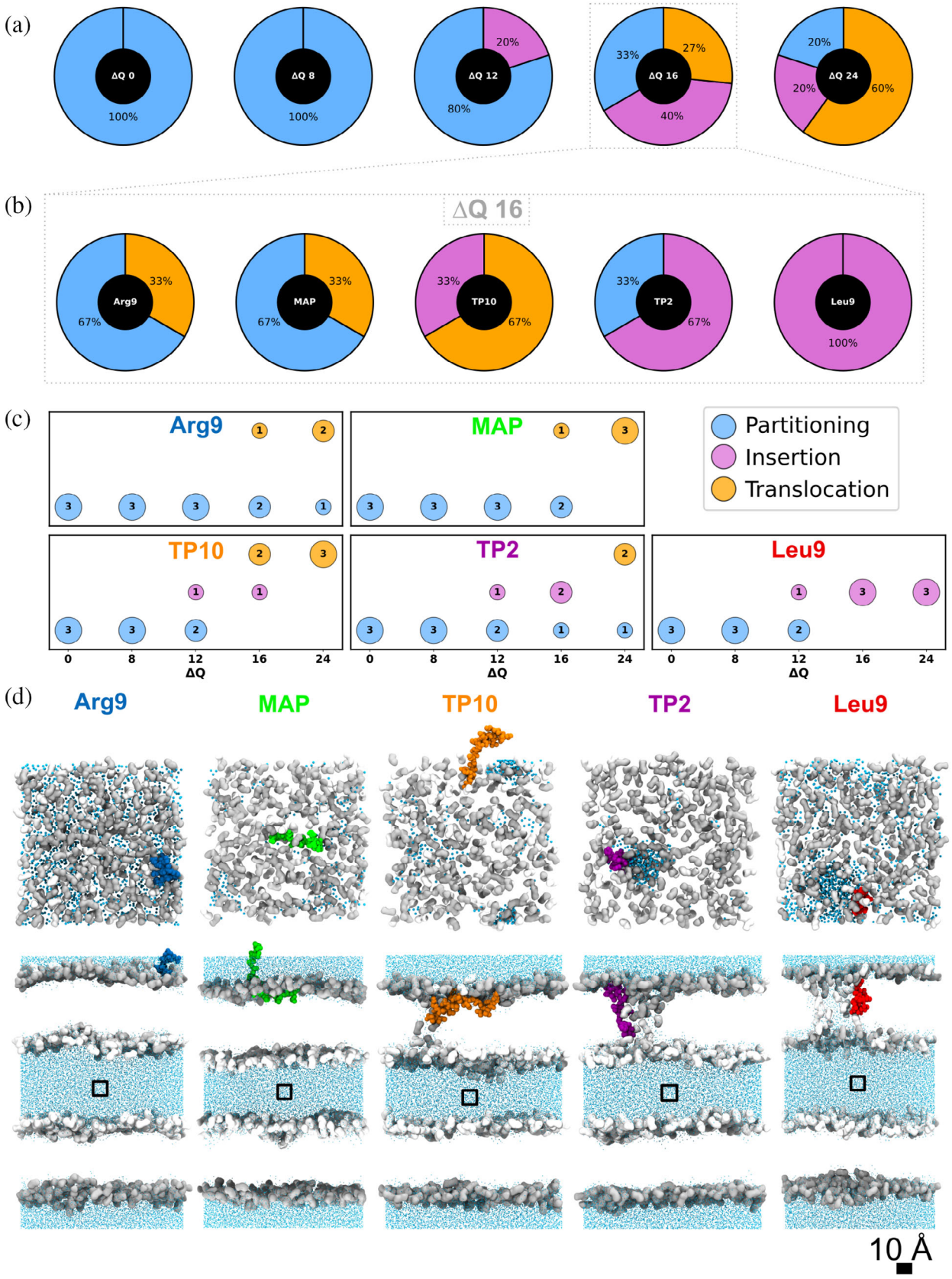

FIGURE 2 Legend on next page.

placing ΔQ/2 K^+ ions in the inner water compartment and the other half by placing ΔQ/2 Cl^- ions in the outer water compartment (Figure 1). We initially ran four sets of 250 ns simulations: at ΔQ 0, 8, 16, and 24, with three replicas for each simulation. However, given the sudden change in simulation outcomes between ΔQ 8 and 16 (see below), we decided to add a new set of simulations, at ΔQ 12, to try to better describe the phenomena occurring.

We decided to use four canonical CPPs: Arg9, MAP, TP10, and TP2 (Table 3). Besides, we chose Leu9 as a negative control, a peptide not expected to present CPP-like capacities due to its high hydrophobicity (Ash et al., 2004). In parallel, we ran a simulation without a peptide, as a membrane-only control. We chose POPC as membrane lipid, since it is extensively used owing to its biological relevance, reliability, and stability in MD simulations and relevance in physiological systems (Ingólfsson et al., 2017). The starting configuration of the peptides and the membranes is presented in Figure 1, where the total number of membrane lipids and water residues is also displayed. Besides, the electron density plot is included, indicating membrane, water, and ion densities.

In order to quantify the potential and electric field generated by the CompEL method, potential and field distributions were calculated using the GROMACS built-in *gmx potential* tool (Figure S1a). Both the transmembrane potential and electric field increase with the imposed charged imbalance, reaching a voltage of approximately 2 V in CompEL ΔQ 16 simulations (the ones selected for detailed analysis, as discussed below). The corresponding electric field across a single membrane averages ~0.3 V/nm (when considering the symmetric double-membrane setup, the net field across the simulation box sums to zero).

In physiological conditions, membrane potentials typically range from ~0 to −150 mV. We therefore emphasize that the membrane potentials applied in this study exceed physiological values. However, the use of elevated transmembrane potentials is a well-established practice in both experimental and computational studies of membrane permeabilization. Experimentally, voltages exceeding ~0.5 V (even though the exact value can vary depending on lipid composition, membrane thickness, and experimental conditions) are known to induce lipid bilayer poration or electroporation (Weaver & Chizmadzhev, 1996). Similarly, MD simulations routinely employ high electric fields or charge-imbalance approaches to induce pore formation or enhance membrane permeability within nanosecond-to-microsecond timescales. In fact, the potential and field values used in this study are similar to those used in other biological studies to induce pore formation through the application of an electric field (Gurtovenko & Vattulainen, 2005; Tieleman, 2004; Tieleman et al., 2003). The application of such elevated potentials in MD compensates for intrinsic timescale limitations of atomistic simulations, enabling the observation of rare membrane remodeling events such as lipid rearrangement, pore nucleation, and peptide insertion within computationally accessible simulation times. The resulting membrane potentials should therefore be interpreted as effective, time-averaged values, rather than as direct representations of experimental or physiological

TABLE 3 Sequence and characteristics of the peptides used in this study. GRAVY score is calculated using the Kyte-Doolittle scale (Kyte & Doolittle, 1982).

Peptide	Length	Sequence	Type	Net charge	GRAVY score
Arg9	9	RRRRRRRRR	Cationic	+9	−4.5
MAP	18	KLALKLALKALKAALKLA	Amphipathic	+5	0.99
TP10	21	AGYLLGKINLKALAALAKKIL	Amphipathic	+4	0.93
Dynorphin A	17	YGGFLRRIRPKLKWDNQ	Amphipathic	4	−1.26
TP2	13	PLIYLRLLRGQWC	Hydrophobic	+2	0.42
Leu9	9	LLLLLLLLL	Hydrophobic	0	3.8
K-FGF	17	AAVALLPAVLLALLAP	Hydrophobic	0	2.42

FIGURE 2 Results in CompEL simulations with one peptide. (a) Illustrative summary of behaviors seen throughout the CompEL simulations in each transmembrane potential through ion imbalance (ΔQ): 0, 8, 12, 16, and 24. We differentiate between peptide partitioning, insertion, and translocation. The results represent the ratio of behaviors of the five peptides (Arg9, MAP, TP10, TP2, Leu9) in the three replicas conducted. Color code: Partitioning in blue, insertion in purple, and translocation in orange. (b) Summary of the outcomes in the simulations of ΔQ 16 differentiating by peptide. (c) Bubble plot of the outcomes for each peptide (y axis), differentiating by the ΔQ (x axis). The size and number inside of each bubble represent the number of each behavior. (d) Molecular representation of the final snapshot in the ΔQ 16 CompEL simulations: Top pose (top image) and side pose (bottom image). Two behaviors are observed: Translocation of Arg9, MAP, and TP10, and insertion with pore formation of TP2 and Leu9. Peptides are colored in its own color, inner membrane in white, outer membrane in gray, and waters in cyan. Peptides are depicted as spheres, and membrane and waters as licorice. Only waters pertaining to the pore are shown in the top pose. Hydrogens are omitted for clarity. A scale bar is added for size clarity. The black box indicates the peptide starting position.

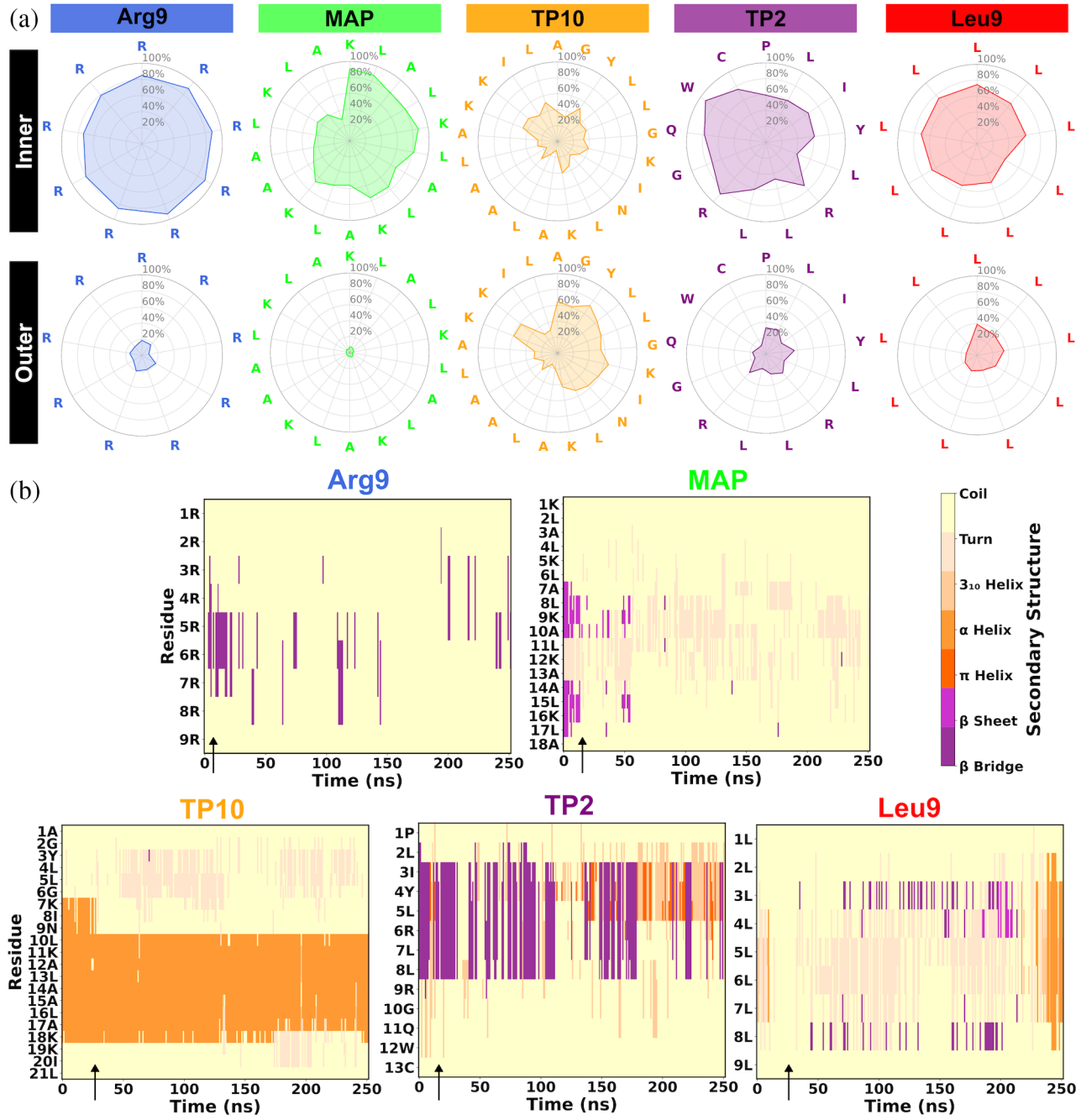

FIGURE 3 Analysis of CompEL ΔQ 16 simulations with one peptide. (a) Radar plot showing the occupancy of each residue with the lipid polar headgroups. Each spoke represents the peptide residue, whereas the radial (inner) axis represents the percentage of occupancy (0–100%). Shaded areas represent the occupancy magnitude for each residue, and higher radial values reflect higher occupancy at the corresponding residue. Lipid occupancy is divided by inner and outer membrane contacts. Residue occupancy is defined as the ratio of simulation time that a residue is in contact with the lipid. The average values for the three replicas are represented. The lipid occupancy referring to the lipid acyl chains is shown in Figure S2. (b) Secondary structure plot. The secondary structure for each residue throughout the simulation is shown. The plot represents the average of the three replicas. The analysis has been done through a tcl script that employed VMD Secondary Structure tool (Humphrey et al., 1996). The arrow indicates the time in which the peptide inserts into the membrane.

values. Importantly, the goal of the present study is not to reproduce absolute physiological membrane potentials, but to compare peptide-specific behaviors under identical electrostatic conditions. By applying the same membrane potential across all systems, we ensure that the observed differences in membrane disruption, insertion, and translocation arise from intrinsic peptide-lipid interactions rather than from variations in the applied field. Consequently, our results should be interpreted in a comparative and mechanistic framework rather than as a direct quantitative prediction of biological membrane behavior.

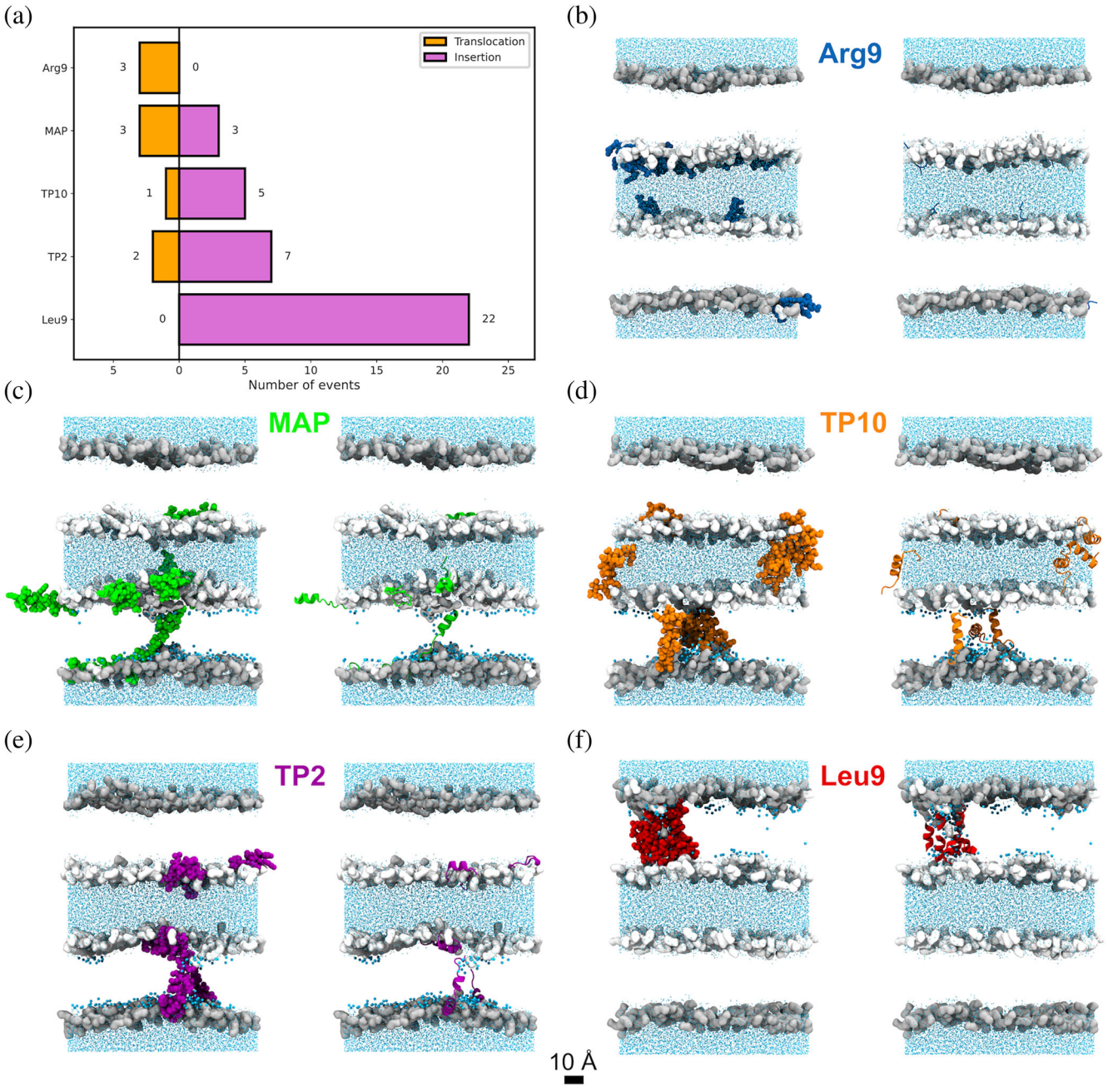

FIGURE 4 Results of CompEL ΔQ 16 simulations with eight peptides. (A) Number of behaviors observed. Only relevant (i.e., translocation and insertion) results are shown. A complete depiction of the results can be seen in Figure S4. The values include the results in the three replicas. (B, C, D, E, F) Molecular representation of the system at the end of the 500 ns of simulation. The peptides represented are Arg9, MAP, TP10, TP2, and Leu9, respectively. Peptides are shown as Van der Waals spheres (left) or cartoon (right). Surface of the polar heads is shown, differentiating between inner (white) and outer (gray) leaflets. Water molecules are shown as licorice, representing in bigger size the water residues in the pore. Hydrogens are omitted for clarity. A scale bar is added for size clarity. Simulation process can be observed in Video S1.

Consistent with experimental electroporation studies, the application of high transmembrane potential leads to pore formation in the membranes. The pore nucleation process observed in control simulations containing only lipid bilayers (simulations without peptides) is described in Figure S1b. Initially, water molecules penetrate into the hydrophobic core of the lipid bilayer, creating transient water defects. This is followed by the nucleation of a water pore through the connection of the inner and outer aqueous compartments. Once formed, the pore supports a continuous flow of water molecules across the membrane. Subsequently, lipid polar headgroups reorient and insert into the pore interior, promoting pore enlargement, until the pore gets stabilized, characterized by a sustained and large water flux and a high density of lipid polar headgroups lining

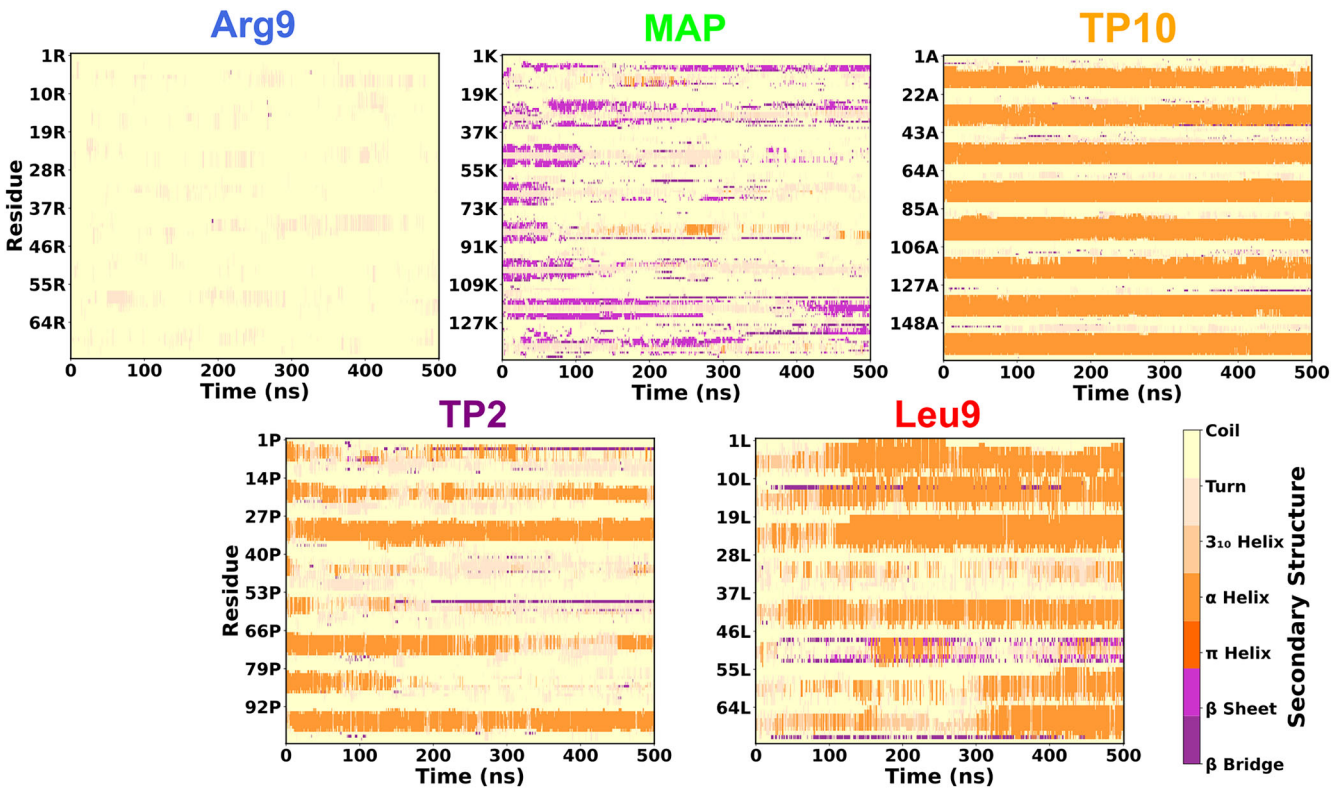

FIGURE 5 Analysis of CompEL ΔQ 16 simulations with eight peptides. Secondary structure analysis is shown, representing the conformation of each of the eight peptides through the 500 ns of the simulation. The plot represents the average structure in all three replicas. The labels in the y-axis indicate the first residue of each peptide.

TABLE 4 Average pore radius (Å) during the 250 ns of CompEL ΔQ 16 simulation. Standard deviation (SD) values are shown. The pore radius is averaged over all frames in the simulation.

# replica	Control	Arg9	MAP	TP10	TP2	Leu9
1	0	31.8 ± 6.7	0.6 ± 0.3	11.5 ± 2.8	4.7 ± 1.9	7.21 ± 0.9
2	24.8 ± 5.5	6.3 ± 2.1	8.2 ± 2.8	3.7 ± 0.6	10.6 ± 2.6	16.8 ± 1.2
3	21.2 ± 5.4	0	0.4 ± 0.2	9.3 ± 1.8	16.7 ± 3.4	20.5 ± 4.1

the pore. These pores get stabilized in a size of ca. 2 nm and can be stable during the whole simulation (see Table 4, membrane-only simulations).

The formation of a pore in the membranes facilitates peptide insertion. However, the interaction of the peptide with the pore and the membrane differs depending on the nature of the peptide. We show the results of each observed behavior for all transmembrane potential simulations (Figure 2a). Among the tested conditions, the ΔQ 16 simulations exhibit the greatest diversity of behaviors and a relatively balanced occurrence for each category, enabling meaningful differentiation between peptides. For this reason, subsequent analyses focus on the ΔQ 16 simulations (Figure 2b). Figure 2c further illustrates the dependence of peptide behavior on the applied ΔQ. Increasing ΔQ results in a higher frequency of insertion and translocation events, supporting the use of higher ΔQ values and underscoring their association with more pronounced membrane-perturbing behaviors.

We classify peptide-membrane interactions into three distinct behaviors. First, inner leaflet adsorption or partitioning: the peptide remains in the inner water compartment while interacting with the inner part of the membrane. Second, insertion (Figure 2d: TP2, Leu9): the peptide uses the pore formed to penetrate the hydrophobic core of the membrane, interacting with lipid polar headgroups on the outer side while remaining in contact with the inner leaflet. In some cases, this state is accompanied by continuous water flux, defining a water pore. Third, outer leaflet stabilization or translocation (Figure 2d: Arg9, MAP, TP10): the peptide not only inserts via the pore but also crosses the membrane, interacting with the outer leaflet and the outer water compartment.

3.2 | CompEL simulations at ΔQ 16

3.2.1 | Peptide analyses

The results of all the simulations, divided by peptide, can be seen in Figure 2b (Table S1). Focusing on ΔQ 16 simulations (Figure 2d), we see how the translocation is the most common result for TP10, whereas Arg9 and MAP partition in most cases, but they also have the ability to translocate the membrane. On the other hand, TP2 and Leu9 are the only peptides that do not show translocation capabilities and get inserted in the membrane in most cases.

Consistent with our simulation results, experimental studies have identified TP10 as a highly efficient translocating peptide across lipid bilayers. In particular, Moghal and collaborators reported that TP10 translocation is strongly enhanced by the presence of a membrane potential, even at relatively low voltages, highlighting the voltage sensitivity of this peptide (Moghal et al., 2020). Notably, those experiments showed that TP10 translocates without permeabilizing the membrane to water-soluble fluorescent probes, indicating that translocation occurs via transient, narrow, and unstable pores or pre-pore states rather than through long-lived, fully water-filled pores.

While the CompEL simulations employed here involve higher effective membrane potentials and stabilize water-filled pores to enable observation of translocation events within accessible timescales, the qualitative agreement is striking: TP10 consistently exhibits the highest translocation propensity among the peptides studied. This suggests that the enhanced translocation of TP10 observed in our simulations reflects an intrinsic peptide property that is also manifested experimentally, even under conditions where pore formation is transient and below the detection threshold for large solutes. Together, these observations support the interpretation that membrane potential facilitates TP10 translocation through electrostatically assisted membrane destabilization, with the nature and lifetime of the permeabilizing defects depending on the magnitude and duration of the applied potential.

Peptide behaviors can also be spotted in Figure 3a, which shows the occupancy of the peptide residues by lipid molecules. Occupancy, analyzed with PyLipID (Song et al., 2022), measures the simulation time in which a residue is in contact with a lipid. In short, Figure 3a shows how peptides interact with POPC membranes. We differentiate between the inner and the outer part of the membrane, and between the interaction with the polar head and the hydrophobic tail of the lipids (see Figure S2a). In this regard, TP10, the peptide that translocates in most cases, shows a higher occupancy in the outer part of the membrane, demonstrating the translocation behavior. On the other hand, in the case of the other four peptides, we see a higher occupancy in the inner part of the membrane. Besides, TP2 and Leu9, the peptides that do not translocate in any replica, also show interaction with the outer leaflet, indicating that the insertion mechanism entails interaction with both leaflets.

Observing the residues that show a higher occupancy, Arg9 and Leu9 show a homogeneous behavior, with a similar occupancy for all residues, given that they are polychains of the same amino acid. Nonetheless, we see a clear difference in the occupancy of these two peptides: Arg9 preferably interacts with POPC polar heads (Figure 3a), whereas Leu9 shows a higher interaction with lipid tails (Figure S2a). These behaviors are explained by the cationic polar nature of arginine, preferably interacting with the negative charge in the phosphate group, and the hydrophobicity of leucine, rather interacting with the hydrophobic lipid tails, respectively (Alaybeyoglu et al., 2016; Lopez et al., 2006). In parallel, in the cases of MAP, TP10 and TP2 we see how, on average, cationic (K, R) or partly polar (Y, N, Q) amino acids show a higher occupancy with the polar heads (Alaybeyoglu et al., 2016) and, conversely, hydrophobic amino acids (L, I, W) preferably interact with the lipid tails (Figure S2a). Interestingly, we see how W12 has a high occupancy with the lipid tails in TP2, which proves that this residue, together with L7-L8, is stabilizing the peptide in the hydrophobic core of the membrane and, therefore, hampering its translocation. In fact, tryptophan was found to strongly interact with the hydrophobic part in the interfacial region of the membrane (MacCallum et al., 2008).

In parallel, peptide secondary structure was analyzed (Figure 3b). We observe that Arg9 and MAP are mostly unstructured during the simulations, as seen in previous studies (Choe, 2023; Oba et al., 2023), TP2 and TP10 remain at a stable structure, and Leu9 is the only peptide where we see a drastic change during the simulation, reaching more than 50% of α-helix structure when it gets inserted in the membrane, phenomena previously described in other studies (Eiríksdóttir et al., 2010; Fiedler et al., 2010; Whitley et al., 2021). TP2 is highly structured in the N-terminal, whereas TP10 shows a higher α-helix percentage in the C-terminal part (Fanghänel et al., 2014). Furthermore, the hydrogen bonds analysis (Figure S2b) shows that Arg9 prefers to interact with lipids, predominantly polar heads as discussed before, which correlates with the lack of secondary structure. On the other hand, Leu9 or TP2 have the highest number of intrapeptide hydrogen bonds, owing to their higher hydrophobicity. Leu9 and TP2, together with TP10, show the highest percentage of secondary structure, again correlated with a higher number of intrapeptide H bonds (Almeida et al., 2012).

3.2.2 | Membrane disruption analysis

An interesting analysis is the pore that is formed in the membranes during the simulations. Transient, small

pores are spontaneously formed in biological membranes (Bennett et al., 2014). In CompEL, owing to membrane stress (Lee et al., 2004) caused by the ion imbalance, pores are also generated without the presence of a peptide (membrane control, Table 4) (Levine & Vernier, 2010; Tarek, 2005), highlighting that peptides are not responsible for pore formation. Still, some of these peptides are able to translocate using the pre-formed pores, as seen in previous studies (He et al., 2015; Park et al., 2024; Sun et al., 2015; Thi Hong Nguyen, 2024).

Lipid order parameter (S_{CH}) analyses have been performed to test the organization and orientation of lipids in the membrane (Figure S3). We see similar results to the ones observed by Ferreira et al. (Ferreira et al., 2013), and thus conclude that the lipids are well-oriented in the membrane. Besides, the application of a transmembrane potential is known to generate lateral membrane tension and bilayer stretching, leading to an increase in the area per lipid. MD simulations of electroporation and charge-imbalance membrane systems have consistently reported bilayer deformation, thinning, and lateral expansion under applied electric fields or ion imbalances (Delemotte & Tarek, 2012; Gurtovenko & Vattulainen, 2005; Leontiadou et al., 2004; Tieleman, 2004). These structural responses arise from electrostatic stress acting on lipid headgroups and are intrinsically linked to pore nucleation and stabilization. The pore formation observed in our CompEL simulations is therefore consistent with previously reported membrane responses to strong electrostatic perturbations.

3.3 | CompEL simulations at higher P:L ratio

Simulations with only one peptide are useful to test the method, but since CPPs do not cross a membrane as individual monomers (Duchardt et al., 2007; Hirose et al., 2012), we simulated the same POPC CompEL system with eight peptides and 256 lipids (per bilayer), corresponding to a 1:32 protein: lipid (P:L) ratio, as in previous studies (Leontiadou et al., 2006). This P:L ratio showed full peptide binding in previous studies (Lee et al., 2013; Magzoub et al., 2002), it was shown to be enough to create stable pore channels for melittin (Irudayam & Berkowitz, 2012) and is close to the ratio used by Herce and Garcia (Herce & Garcia, 2007) in the study with Tat peptides (1:18). Besides, more peptides would require larger water compartments, and we wanted to keep the same system conditions as for one peptide.

Three replicas of CompEL 250 ns simulations were run for ΔQ 0, 8, 12, and 16. ΔQ 24 was discarded in order to reduce the electric field applied to the system. As in the CompEL simulations with one peptide, the ΔQ 16 simulations presented the possibility of observing peptide translocation and were consequently used for simulation analysis (Figure 4 and Video S1). System stabilization was not achieved with 250 ns (as shown by the RMSD analysis, Figure S5), thus the ΔQ 16 simulations were extended to 500 ns. The global results seen for ΔQ 0, 8, and 12 can be seen in Figure S4 and Table S2.

3.3.1 | Peptide analysis

As shown in Figure 4a, Table S2, and Video S1, the results reveal different translocation and insertion behaviors among the peptides. From a total of eight peptides, one Arg9 peptide is able to translocate in each replica, achieving a total of three translocation events in total in the three replicas. MAP shows one translocation and one insertion in each replica, with a total of three translocations and three insertions among the three replicas. Thus, Arg9 and MAP were the peptides with the highest translocation ratio, as reported in experimental studies, where it was shown that Arg9 and MAP are CPPs with high efficiency (Liu et al., 2012; Mo et al., 2011). For TP10, only one TP10 translocates in one replica, whereas in the other two replicas, 2 and 3 TP10 peptides get inserted in the membrane. For TP2, which showed no translocation capacity in simulations with one peptide, one TP2 peptide is now able to translocate in two replicas, with a total of two translocation and seven insertion events in the three replicas, confirming TP2 ability to translocate symmetric phospholipid membranes (Cruz et al., 2013). Last, as in simulations with one peptide, Leu9 does not show translocation capacity, but it does show insertion behavior, with 22 peptides getting inserted across the three replicas. In short, ΔQ 16 simulations demonstrate the CPP behavior of the four CPPs used in the study, whereas Leu9, the negative control without CPP characteristics, can get inserted but has no translocation capacity.

At the molecular level (Figure 4b–f), Arg9 peptides show two possible behaviors: partitioning, where they get adsorbed to the inner leaflet and interact with the polar heads, or translocation, where they cross the membrane and interact with the polar heads in the outer leaflet. In both cases, Arg9 peptides interact with POPC polar heads, owing to the positive charges in Arg9's structure and negative charges in the polar heads, as discussed previously. The opposite behavior is seen for Leu9 peptides, which mostly get inserted in the membrane, preferring the interaction with the hydrophobic lipid tails. The other three CPPs (MAP, TP10, TP2) have hydrophobic, polar, and charged amino acids in their structure and can, therefore, interact with the polar heads in the partitioning and translocation behaviors, or get inserted and interact with the aliphatic lipid chains.

Regarding the secondary structure (Figure 5), we see similar results to the ones discussed for

TABLE 5 Average ratio of intra-peptide H bonds formed during the 3 replicas of 500 ns of CompEL ΔQ 16 simulations with 8 peptides.

H bonds	Arg9	MAP	TP10	TP2	Leu9
Average	82.5 ± 0.7	60.7 ± 3.5	57.8 ± 4.2	51.7 ± 4.9	51.8 ± 1.9

Note: Standard error of the mean (SEM) values are shown.

simulations with one peptide (Figure 3b), with Arg9 mainly unstructured, most MAP peptides unstructured, even though some showed β-sheet structure, TP10 with a stable α-helix structure in the C-terminal, and Leu9 gaining secondary structure owing to the membrane insertion (Eiríksdóttir et al., 2010; Fiedler et al., 2010; Whitley et al., 2021). Only TP2 shows considerable differences, since it changes from β-sheet to α-helix, with most peptides unstructured during the simulation, which can be related to a higher partitioning or translocation behaviors and, therefore, lower insertion ratio, typically associated with α-helix formation, as seen for Leu9.

Comparing these results with the simulations containing a single peptide, an overall increase in translocation or insertion events is observed, highlighting the importance of peptide number for translocation capacity (He et al., 2015; Muñoz-Gacitúa et al., 2022; Oba et al., 2023). However, the effect of increased peptide concentration is peptide-dependent and reflects distinct underlying mechanisms. In systems containing Arg9, the higher number of translocation events is primarily a consequence of the increased number of peptides available to exploit transient membrane defects or pores, rather than enhanced peptide–peptide cooperativity. In fact, Arg9 peptides display minimal inter-peptide interactions (Figure 4b; Choe, 2023; Sun et al., 2014; Thi Hong Nguyen, 2024; Thi Hong Nguyen & Vazdar, 2024) and predominantly form hydrogen bonds with lipid headgroups (Figure S6). Consistently, Arg9 exhibits a high proportion of intra-peptide hydrogen bonds (∼80%, Table 5), indicating that Arg9 peptides remain largely monomeric while translocation occurs, even in multi-peptide systems.

Conversely, the other peptides do show cooperativity behavior, supported by a higher inter-peptide H bond ratio (Figure S6 and Table 5), in line with previous reports (Fanghänel et al., 2014). This cooperativity manifests differently depending on the peptide. MAP peptides exhibit an increased number of translocation events compared to the single-peptide system, an effect primarily attributable to the higher number of peptides available to cross the membrane through the ΔQ-induce pore rather than to enhanced peptide–peptide cooperativity. Still, MAP peptides show higher cooperativity capacity compared to Arg9 (Figure S6 and Table 5), confirming the amphipathic nature of MAP, capable of interacting with polar heads and lipid acyl chains, and among themselves. In fact, the hydrophobic part of the peptide is corroborated by the capacity to get inserted in the membrane and get stabilized without the presence of the pore, just by interacting with the hydrophobic core of the membrane (Figures 4c and S7).

Interestingly, this cooperative behavior can also reduce translocation probability for certain peptides. TP10 shows a reduction in translocation events in the multi-peptide simulations despite the higher peptide number. This behavior correlates with an increased propensity for peptide–peptide interactions (Figure S6), favoring stable aggregates at the membrane interface and within the bilayer. In this case, the presence of multiple peptides favors mutual stabilization through inter-peptide hydrogen bonding (Table 5), leading to a competition between cooperative insertion and peptide translocation. Consequently, TP10 peptides tend to remain interacting and organized as clusters (Figures 4d and S7), which limits their ability to cross the membrane. These results suggest that, for TP10, increased peptide concentration shifts the balance from translocation toward cooperative membrane association.

TP2 shows a clear cooperative behavior in the eight-peptide simulations, characterized by a substantial increase in inter-peptide hydrogen bonds and stable peptide aggregates (Table 5 and Figures 4e and S7). Unlike Arg9, TP2 relies on peptide–peptide interactions to achieve membrane insertion, and this cooperative assembly plays a central role in its interaction with the bilayer. Moreover, cooperativity also helps to achieve peptide translocation, as the hydrophobicity of TP2 allows the peptides to get inserted and stabilized in the bilayer, and the polar amino acids facilitate the interaction with the polar headgroups in the lower leaflet, which leads to translocation.

Finally, Leu9 peptides show a strong tendency to self-assemble (Figure S6), which facilitates their insertion in the membrane (Illya & Deserno, 2008). Leu9 displays the highest self-assembly propensity (Table 5), preferentially interacting with other peptides and with lipid acyl chains. As shown in Figure S7, Leu9 aggregates contribute to pore stabilization, with polar atoms (N, O) oriented toward the aqueous phase while carbon atoms face the hydrophobic lipid tails.

Altogether, these observations point to at least two distinct mechanistic classes of CPP behavior in multi-peptide systems: a predominantly monomeric, lipid-mediated translocation mechanism exemplified by Arg9, and a cooperative, aggregation-driven mechanism characteristic of peptides such as TP10 and TP2.

TABLE 6 Average pore radius (Å) during the 500 ns of CompEL ΔQ 16 simulation with 8 peptides.

# Replica	Arg9	MAP	TP10	TP2	Leu9
1	6.2 ± 1.5 1 peptide	6.2 ± 1.6 1 peptide	11.5 ± 2.2 3 peptides	4.7 ± 1.2 2 peptides	15.5 ± 2.3 7 peptides
2	5.3 ± 1.4 1 peptide	5.5 ± 1.4 1 peptide	5.7 ± 1.6 1 peptide	10.6 ± 2.1 3 peptides	20.1 ± 2.7 8 peptides
3	6.0 ± 1.5 1 peptide	5.7 ± 1.5 1 peptide	9.3 ± 1.8 2 peptides	16.7 ± 2.3 3 peptides	24.7 ± 3.8 7 peptides
Average	5.3 ± 0.5	5.8 ± 0.5	8.8 ± 0.9	10.7 ± 0.8	20.1 ± 1.6

Note: SD values are shown. The pore radius is averaged over all frames in the simulation. The second line indicates the number of peptides involved in pore formation in each replica.

3.3.2 | Membrane disruption analysis

Table 6 shows the pore analyses conducted for ΔQ 16 simulations with eight peptides. Arg9 and MAP do not contribute to the pore persistence, but TP10, TP2, and specially, Leu9 are able to stabilize it. This behavior is depicted in Figure S7, where we see how one MAP peptide is inserted in the bilayer, but does not allow water flow, opposite to TP10, TP2, and Leu9, which cooperate and are able to stabilize the pore. Interestingly, the nature of the pores differs between simulations containing one and eight peptides. In simulations with a single peptide, lipid polar headgroups show a high degree of involvement in pore formation (Figures 4d and S8), resulting in a pore with a toroidal-like nature (Sengupta et al., 2008; Yang et al., 2001). In contrast, in simulations with eight peptides, lipid molecules contribute less to pore stabilization, while peptides play a dominant role, giving rise to a barrel-stave-like pore character (Figures 4d–f, S7, and S8) (Yang et al., 2001).

These simulations have also allowed us to observe lipid flip flop from the inner to the outer leaflet in systems containing peptides (Figure 5B–F). Lipid flip-flop occurs concomitantly with peptide translocation across the water channel (Choe, 2023; Leontiadou et al., 2006; Muñoz-Gacitúa et al., 2022; Tieleman & Marrink, 2006; Vernier et al., 2006), and preferentially from peptide-enriched to peptide-free bilayers (Leontiadou et al., 2006). Contrastingly, no lipid flip-flop events have been observed in peptide-free control simulations over the timescales sampled. This observation is consistent with previous studies suggesting that membrane-active peptides can facilitate lipid flip-flop by transiently stabilizing polar headgroups during peptide insertion or translocation, or by perturbing bilayer structure (Nguyen et al., 2019).

3.4 | Translocation and insertion mechanisms

Snapshots illustrating representative translocation (Arg9, Figure 6a–g) and insertion (Leu9, Figure 6h–m) events are shown in Figure 6. The representative snapshots of MAP, TP10, and TP2 processes are shown in Figure S9. The sequence of pore formation and annihilation is compared follows the stages described by Levine & Vernier and can be consistently divided into pore initiation, pore construction, pore maturation, and subsequent degradation and deconstruction (Levine & Vernier, 2010).

In the Arg9 simulations, translocation proceeds through a four-step process. First, pore initiation occurs through the formation of a water defect that connects the two aqueous compartments (Figure 6b). As discussed above, this step is induced by the transmembrane potential and is not directly driven by peptide action. Second, during pore construction (Figure 6c), lipid polar headgroups from opposing leaflets migrate toward the defect, followed by pore maturation (Figure 6d), characterized by a large number of waters and stabilization by lipid headgroups. At this stage, Arg9 peptides are attracted to the electrostatically favorable pore environment. Third, a peptide inserts into the membrane through the matured pore (Figure 6e) and remains associated with it for approximately 300 ns. Finally, the peptide crosses to the outer leaflet, coinciding with the process of pore annihilation (Figure 6f). Pore closure involves (i) pore degradation, when water molecules and polar heads start to migrate out of the bilayer and the pore starts to thin, followed by (ii) pore deconstruction, defined by the absence of headgroup participation. Fourth and last, the Arg9 peptide has crossed the bilayer and stabilized in the outer leaflet, triggering pore dissolution (Figure 6g) and completing pore annihilation, when all water molecules are expulsed from the membrane. Comparing the average pore sizes of membrane-only control simulations (Table 4) and simulations with eight Arg9 peptides (Table 6), it is seen how Arg9 translocation leads to a decrease in average pore size, indicating that peptide translocation and pore closure are related.

The MAP translocation mechanism (Figure S9) follows the same sequence of pore initiation, construction, and maturation induced by the applied transmembrane potential. Upon pore maturation, a MAP peptide inserts into the membrane and subsequently translocates.

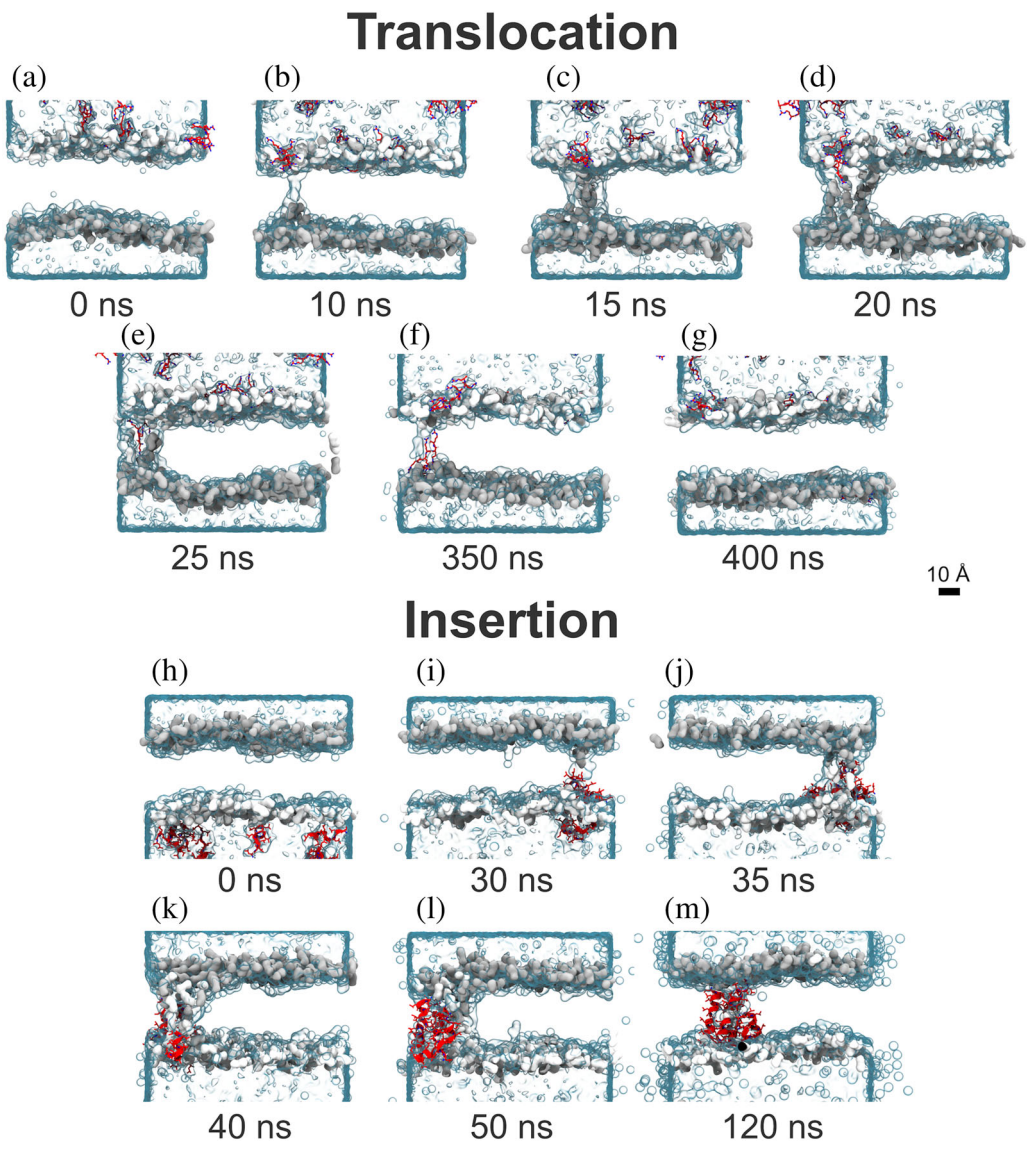

FIGURE 6 1. Arg9 translocation procedure in CompEL ΔQ 16 simulation with 8 peptides. Representative snapshots illustrate the structural organization of the membrane during the translocation process, portraying the key steps: (a) simulation start, some peptides adsorb to the bilayer surface, (b) pore initiation, with water molecules entering in contact, (c) pore construction, the polar heads from both bilayers interact, (d) pore maturation, with polar heads connected, resulting in a larger pore; a peptide gets attracted to the pore and starts the insertion, (e) one peptide gets inserted into the pore, (f) the peptide reaches the outer leaflet, causing pore deconstruction, with no more interactions between polar heads, and (g) the peptide finalizes the translocation and stabilizes into the outer leaflet, leading to pore dissolution. 2. Leu9 insertion procedure in CompEL ΔQ 16 simulation with 8 peptides. (h) Start of the simulation, (i) Pore initiation, and peptide insertion, (j) Pore construction, (k) Pore maturation, (l) More peptides insertion, and (m) Eight peptides insertion. Arg9 and Leu9 peptides are colored in red and represented as Cartoon, while showing the sidechain atoms (C in red, N in darker blue, O in white). The polar heads surface is shown and colored based on the bilayer: Inner in white, outer in gray. Water molecules are shown as transparent cyan surface. Lipid tails are omitted for clarity. The insertion and translocation processes of the other CPPs (MAP, TP10, and TP2) are shown in Figure S9.

Notably, due to its amphipathic nature, MAP can interact not only with waters molecules and polar headgroups, but also with the hydrophobic core of the membrane. This facilitates insertion even as the pore undergoes degradation and deconstruction, resulting in a reduction of the average pore size compared to control simulations (Tables 4 and 6). After pore closure, MAP remains stabilized within the membrane, interacting with polar headgroups from both leaflets. This stable insertion correlates with a transition toward an α-helical conformation, consistent with previous reports (Fiedler et al., 2010; Whitley et al., 2021).

In TP10 simulations (Figure S9), the early stages of pore initiation, construction and maturation are comparable to those observed for Arg9 and MAP. Following pore maturation, three TP10 peptides insert into the membrane through the stabilized pore. Similar to MAP, TP10 peptides adopt a stable α-helical conformation upon

insertion. Peptide insertion is accompanied by a decrease in the average pore size (Tables 4 and 6), but it does not lead to pore closure. Experimental studies have reported a multi-step mechanism for TP10-membrane interactions in the absence of applied membrane potential. At high peptide-to-lipid ratios, TP10 was shown to first translocate across lipid bilayers without detectable formation of stable pores, leading to peptide accumulation at both membrane interfaces, and only subsequently inducing membrane permeabilization to large fluorescent probes (Islam et al., 2014). This behavior suggests that translocation can occur through transient, narrow, or unstable defects that do not allow passage of larger solutes. A similar sequential process has been described for melittin, where peptide redistribution between leaflets precedes cooperative pore formation (Lee et al., 2013). In our CompEL simulations, translocation events are tightly coupled to the formation of water-filled pores, as the applied transmembrane potential promotes defect stabilization. Therefore, while our simulations capture pore-enabled peptide transport and cooperative effects at higher peptide numbers, they do not fully resolve the early, transient, or non-classical intermediates proposed experimentally. The comparison suggests that TP10-induced pore formation is likely a concentration- and symmetry-dependent cooperative process, and that CompEL preferentially samples the pore-stabilized branch of this mechanistic landscape.

For TP2 (Figure S9), pore initiation, construction, and maturation again precede peptide insertion. Three TP2 peptides insert into the membrane via the matured pore. In one case, insertion progresses to full translocation, with the peptide interacting with polar headgroups of the outer leaflet and stabilizing in that leaflet. As observed for other peptides, insertion promotes pore degradation, leading to stabilization of a reduced pore size (Table 6) (Cruz et al., 2013).

Leu9 exhibits a distinct behavior characterized predominantly by an insertion rather than full translocation (Figure 6h–m). Following pore initiation (Figure 6i), a peptide positioned near the defect rapidly participates in pore construction (Figure 6j), and insertion occurs concomitantly with pore maturation (Figure 6k). Subsequently, additional peptides are attracted to the pore and insert into the membrane (Figure 6l), with all peptides stabilizing the pore after the first 120 ns of the simulation (Figure 6m). In contrast to other systems, multiple Leu9 peptides stabilize the matured pore, preventing pore degradation and deconstruction, resulting in a long-lived, peptide-stabilized pore that persists for the remainder of the 500 ns simulation.

Across all systems, peptide orientation follows a consistent pattern: peptides are initially oriented parallel to the membrane during peptide partitioning, reorient perpendicularly during insertion, and they finally adopt a parallel orientation again upon translocation, consistent with previous observations (Leontiadou et al., 2006).

Several experimental and theoretical studies have proposed the pre-pore model to explain CPP translocation across lipid bilayers. In this framework, peptides cross the membrane through transient, nanoscale defects generated by thermal fluctuations in lipid packing (Hasan et al., 2019; Moghal et al., 2020). These pre-pores are typically short-lived and narrow, as their expansion is energetically limited by the line tension at the pore. In tension-free membranes, such defects are rare and rapidly close; however, increases in membrane tension (either due to external forces, peptide binding, or applied electric fields) enhance both the frequency of defect formation and their effective radius (Islam et al., 2017). In the present CompEL simulations, peptide translocation does not occur through a transient, subcritical defect but rather through a fully developed, water-filled pore. Following pore initiation, pore construction and maturation lead to a continuous aqueous channel stabilized by lipid headgroups. This pore remains stable in membrane-only control simulations (Table 4) and during peptide insertion (Table 6, Leu9), whereas it collapses in some cases where translocation occurs (Table 6, Arg9, and MAP). Thus, the conductive structure observed here differs from the classical short-lived pre-pore described in tension-free systems. Nevertheless, the two mechanisms may be mechanistically related. The applied transmembrane potential in CompEL increases membrane stress and can stabilize lipid packing defects that would otherwise remain transient. In this sense, the observed conductive pore may represent a voltage-stabilized analogue of a pre-pore, where a stable transmembrane channel enables peptide insertion and translocation within the simulated timescale.

As discussed above, when a CPP completes translocation, it promotes pore closure (He et al., 2015; Huang & García, 2013; Sun et al., 2014) (Figure 6d), characterized by water and lipid headgroups expulsion from the membrane hydrophobic core (Levine & Vernier, 2010), as observed for Arg9 and MAP, which exhibit the smallest average pore sizes (Table 6). Moreover, TP10 only translocates in the second replica (Table S2), precisely the one in which pore closure occurs (Table 6), confirming the relationship between these two events. TP2 also shows translocation in two of the replicas, but pore closure is not seen, which can be related to the TP2 lower net charge (+2), possibly not being enough to reduce the transmembrane potential under the pore-forming threshold. Still, we hypothesize that in longer timescales, more TP2 peptides are able to translocate, ultimately inducing pore closure (we extended the TP2 simulations to 1 μs, but no significant changes were observed, so larger timescales may be needed), as TP2 has been seen to translocate without inducing strong bilayer perturbations (Cruz et al., 2013). Within the framework of the pre-pore model, peptide insertion appears to transiently stabilize a voltage-induced pore, while completion of

translocation seems to trigger pore collapse, ensuring bilayer integrity. We note that the precise contribution of charge imbalance to pore lifetime seems to be important, and further work including more variables, such as different membrane compositions, membrane asymmetry studies should be pursued, and direct experimental validation remains an important direction for future work.

3.5 | CompEL discussion

In the CompEL simulations, we have seen how CPPs are able to use the pores formed due to ion imbalance to internalize (Sun et al., 2014, 2015). In short, the four CPPs have demonstrated translocation capabilities, as opposed to our previous CPP study (Catalina-Hernandez, Aguilella-Arzo, et al., 2025), where only Arg9 (TP10 was not studied) was able to achieve translocation. In this sense, we have seen how CPP translocation can occur through pore formation, leading to pore closure and potentially explaining the lack of cell toxicity of CPP translocation (Trofimenko et al., 2021). On the other hand, Leu9 causes larger pore sizes, marking the difference compared to peptides with CPP characteristics, since Leu9 peptides are not able to translocate and they are indeed able to stabilize the pore, a behavior correlated with other bioactive peptides such as antimicrobial peptides (AMPs) (Leontiadou et al., 2006).

An apparent discrepancy between simulations and experiments is that no peptide insertion or translocation events were observed at ΔQ 8, despite the corresponding membrane potential being substantial (Figure S1), whereas experimental studies report that the relatively low membrane potential ($\sim$100 mV) significantly enhance peptide-induced pore formation and CPP translocation rates (Moghal et al., 2020; Rashid et al., 2020). This difference likely reflects fundamental distinctions between atomistic MD simulations and experimental system rather than a reduced effectiveness of membrane potential in CompEL. First, pore nucleation is a stochastic rare event. In experiments, membrane potentials act over millisecond-to-second timescales and across micron-scale membrane areas, greatly increasing the probability of defect formation. In contrast, atomistic MD simulations are limited to nanosecond-to-microsecond timescales and nanometer-scale membrane patches, requiring stronger electrostatic perturbations to observe pore formation within accessible computational times. Second, biological membranes are structurally heterogeneous and may contain pre-existing curvature stress, compositional asymmetry, or protein-induced defects that make pore nucleation more likely. Such factors are absent in the symmetric, protein-free bilayers employed here. Finally, CompEL imposes a global charge imbalance across a periodic double-membrane system, whereas in vivo membranes may experience localized and transient electric fields that can concentrate electrostatic stress in restricted regions. Taken together, these differences likely explain why higher effective membrane potentials are required in simulations to trigger pore-mediated insertion and translocation events. Therefore, our results should be interpreted in terms of mechanistic trends under controlled electrostatic stress rather than as a direct quantitative mapping to experimental voltage thresholds.

Charge seems to be an important factor in deciding translocation, so simulations containing K-FGF (Lin et al., 1995), a neutral CPP, and Dynorphin A (Fischli et al., 1982; Smith & Lee, 1988), a positively charged peptide that did not show internalization behavior in our last study (Catalina-Hernandez, Lopez-Martin, et al., 2025) (Table 3), have been run. Both systems containing eight peptides and ΔQ 16 showed no translocation behaviors, with only insertion or partitioning in both cases (Figure S10). Therefore, we can conclude that the charge is not the sole determinant of the translocation process in CompEL.

Another determinant in the translocation process is membrane composition. All simulations in this study were performed using symmetric, zwitterionic POPC bilayers, which provide a well-defined reference system for methodological development. However, it is well established that CPP-membrane interactions and translocation efficiency are highly sensitive to lipid composition, including the presence of negatively charged lipids, cholesterol content, and membrane asymmetry (Alves et al., 2008; Sharmin et al., 2016; Zakany et al., 2023). Accordingly, the present results should be interpreted as a proof-of-concept demonstrating the applicability of the CompEL approach to study CPP-induced membrane perturbations, rather than as a comprehensive description of CPP behavior in physiologically realistic membranes or as a direct representation of endosomal escape in vivo. Nonetheless, the peptide-specific differences observed here suggest that intrinsic physicochemical properties (charge density, amphipathic nature, hydrophobic content) may differentially regulate membrane destabilization across distinct biological membranes. Extending this framework to charged, cholesterol-containing, and asymmetric bilayers represents an important direction for future studies, whereas CompEL simulations using endosomal-like lipid compositions could help elucidate how membrane context modulates CPP behavior during endosomal escape (Madani et al., 2011; Magzoub et al., 2005).

In conclusion, the CompEL approach provides a robust and physically motivated framework to study membrane processes under an applied transmembrane potential. According to the CPP translocation process (Herce & Garcia, 2007; Yandek et al., 2007), peptides adsorb or partition to the inner leaflet. They

then destabilize the membrane while attempting to reach the polar heads in the outer leaflet, ultimately causing pore formation and allowing peptide translocation. However, it is challenging to observe pore formation in cMD, owing to the energetic cost of the process (Bennett et al., 2014). Precisely, by imposing a charge imbalance between aqueous compartments, CompEL generates a self-consistent membrane potential without the need for an external electric field, allowing ions, water, lipids, and solutes to respond dynamically. This method has been applied to investigate electroporation, membrane permeability, and peptide-membrane interactions, offering a direct way to probe voltage-dependent phenomena while maintaining full atomistic resolution. In addition, CompEL enables comparative analyses under well-defined electrostatic conditions, making it particularly suitable for identifying relative trends across systems or perturbations, thus enabling the observation of unbiased translocation of CPPs.

At the same time, CompEL has intrinsic limitations that must be considered when interpreting the results. In particular, the applied charge imbalance typically leads to pore nucleation at sufficiently high potentials, such that translocation events observed in CompEL simulations necessarily occur via pore-mediated mechanisms. As a consequence, alternative translocation pathways that may operate under lower or transient membrane potentials, such as direct peptide insertion, non-pore-mediated mechanisms or energy-dependent mechanisms, are not explicitly captured. Moreover, as with other voltage-driven MD approaches, the membrane potentials required to observe rare events within accessible simulation times exceed physiological values, and results should therefore be interpreted in a comparative and mechanistic rather than quantitative physiological framework. Despite these limitations, CompEL remains a powerful tool for dissecting voltage-dependent membrane perturbation mechanisms when its scope and assumptions are clearly defined.

While the transmembrane potentials applied in this study exceed physiological membrane potentials, it is important to distinguish between global applied voltages and local electric fields experienced by membranes in biological contexts. Local electric fields of comparable magnitude can arise transiently from charge separation, molecular dipoles, and asymmetric distributions of charged residues, particularly in confined environments such as endosomal membranes. Recent work has highlighted the role of peptide dipoles and local electrostatic effects in promoting membrane destabilization and endosomal escape, without invoking a sustained global membrane potential (Batta et al., 2021).

In this context, the present CompEL simulations are not intended to reproduce physiological electric field directly, but rather to provide mechanistic insight into how strong electrostatic stress, whether arising from applied potentials or local charge imbalances, couples to membrane deformation, pore formation, and peptide translocation. Our results therefore emphasize general physical principles underlying voltage-assisted membrane perturbation, while physiological relevance should be interpreted in terms of transients, localized electrostatic effects rather than sustained macroscopic membrane potentials.

4 | CONCLUSIONS

In this study, we have performed CompEL simulations to study CPP behavior under applied potential in model lipid membranes. The first step in CPP translocation through pore formation is the peptide adsorption to the membrane, destabilizing the membrane and allowing pore formation, which the CPPs will use to translocate. However, to observe the complete translocation in cMD simulations is cumbersome, owing to the energetic cost of pore formation. Precisely, CompEL enhances pore formation via ion imbalance in the membrane, allowing the computational study of CPP translocation.

In short, in ΔQ 16 CompEL simulations with one peptide, TP10 showed the highest translocation capacity, followed by Arg9 and MAP, with TP2 and Leu9 not showing internalization behavior. More translocation events were seen in ΔQ 16 CompEL simulations with eight peptides, where Arg9 and MAP showed the highest translocation capacity, followed by TP2 and TP10. Moreover, CompEL simulations have also revealed that once pores spontaneously form in the cell membrane under charge imbalance conditions, peptides can stabilize them (such as Leu9) or translocate through them (such as Arg9, MAP, TP10, or TP2).

We present CompEL, a method with significantly lower computational requirements compared to US, where up to 4 μs (Huang & García, 2013) are needed. Besides, CompEL is entry-level, easier to parallelize, and less GPU-intensive than aSMD (Catalina-Hernandez, Aguilella-Arzo, et al., 2025). In this study, simulations at several ΔQ values were required to perform method calibration, but in subsequent studies, simulations at only one ΔQ (e.g., ΔQ16) need to be run, considerably decreasing the overall computational cost. Additionally, CompEL increases the feasibility of performing replicas and allows simulations with a higher number of peptides, being able to analyze peptide cooperativity or aggregation. Moreover, CompEL is an enhanced molecular dynamics technique, but, contrary to aSMD or US, in CompEL the peptide is not forced to translocate the membrane; rather it provides an unbiased exploration of the peptide-membrane interaction. Thus, CompEL can be used to describe at the molecular level the peptide interaction with the membrane, and with higher resolution than coarse-graining methods. Simulations using a potential difference and a single membrane can be conducted, but peptides may

translocate to the opposite membrane via the PBC, which is prevented in CompEL, enabling the encapsulation of peptides between two membranes, which also simplifies analysis and enhances control over the system.

We believe that this study can be a first step in the use of CompEL for CPPs computational research. However, CompEL simulations only account for CPP translocation via pore formation, whereas CPPs can internalize through additional mechanisms, as discussed above. In this study, each condition was simulated using three independent replicas, which is sufficient to identify robust qualitative trends but may limit sampling of rare stochastic events such as pore formation and peptide translocation. Accordingly, reported differences in CPP efficiency should be interpreted as relative trends, and the absence of observed translocation reflects limited sampling within the simulated time window rather than its impossibility. Besides, while we have conducted simulations with symmetric, neutral, zwitterionic POPC bilayers, future work should explore negatively charged bilayers (e.g., containing PS or PG), more physiologically relevant compositions (e.g., asymmetric containing phosphatidylethanolamine or cholesterol), and comparison with experimental studies in order to perfect this technique. Lastly, CompEL requires the application of a high voltage, which necessitates cautious interpretation of the results. Additional simulations may be needed to further increase the sampling of the systems, possibly combining CompEL with elevated temperatures to increase molecular mobility. Future studies should also investigate different P:L ratios to assess the influence of P:L ratio in CPP internalization.

In conclusion, we propose the use of CompEL to computationally study CPP insertion or translocation at a molecular level, which is challenging to achieve with other techniques. Furthermore, CompEL can be expanded to study the interaction of other types of membrane-active peptides, such as AMPs, antiviral, or anticancer peptides.

AUTHOR CONTRIBUTIONS

Eric Catalina-Hernandez: Writing – original draft; writing – review and editing; conceptualization; investigation; formal analysis; methodology. **Marcel Aguilella-Arzo:** Writing – review and editing; funding acquisition; resources; formal analysis; methodology; visualization. **Mario Lopez-Martin:** Writing – review and editing; supervision; formal analysis. **Alex Peralvarez-Marin:** Conceptualization; writing – review and editing; funding acquisition; supervision; project administration; visualization; formal analysis; methodology; resources.

ACKNOWLEDGMENTS

Authors acknowledge financial support by the Spanish Government Grant PID2020-120222GB-I00 (to Alex Peralvarez-Marin) and PID2022-142795NB-I00 (to Marcel Aguilella-Arzo) funded by Ministerio de Ciencia Innovacion y Universidades 10.13039/501100011033, Ministerio de Universidades Ciencia Innovacion y Universidades Margarita Salas Award (MGSD2021-10 to Mario Lopez-Martin) and Universitat Autònoma de Barcelona predoctoral fellowship (B21P0033 to Eric Catalina-Hernandez) and Universitat Jaume I project UJI-B2022-42 (to Marcel Aguilella-Arzo).

CONFLICT OF INTEREST STATEMENT

The authors declare no conflict of interest or competing interest.

DATA AVAILABILITY STATEMENT

The data that support the findings of this study are available from the corresponding author upon reasonable request.

ORCID

Eric Catalina-Hernandez https://orcid.org/0009-0007-6365-6292
Marcel Aguilella-Arzo https://orcid.org/0000-0002-2831-455X
Mario Lopez-Martin https://orcid.org/0000-0001-5496-9827
Alex Peralvarez-Marin https://orcid.org/0000-0002-3457-0875

REFERENCES

Abraham MJ, Murtola T, Schulz R, Páll S, Smith JC, Hess B, et al. GROMACS: high performance molecular simulations through multi-level parallelism from laptops to supercomputers. SoftwareX. 2015;1:19–25. https://doi.org/10.1016/J.SOFTX.2015.06.001

Alaybeyoglu B, Sariyar Akbulut B, Ozkirimli E. Insights into membrane translocation of the cell-penetrating peptide pVEC from molecular dynamics calculations. J Biomol Struct Dyn. 2016; 34(11):2387–98. https://doi.org/10.1080/07391102.2015.1117396

Almeida PF, Ladokhin AS, White SH. Hydrogen-bond energetics drive helix formation in membrane interfaces. Biochim Biophys Acta. 2012;1818(2):178–82. https://doi.org/10.1016/J.BBAMEM.2011.07.019

Alves ID, Goasdoué N, Correia I, Aubry S, Galanth C, Sagan S, et al. Membrane interaction and perturbation mechanisms induced by two cationic cell penetrating peptides with distinct charge distribution. Biochimica et Biophysica Acta (BBA) - General Subjects. 2008;1780(7–8):948–59. https://doi.org/10.1016/j.bbagen.2008.04.004

An M, Wijesinghe D, Andreev OA, Reshetnyak YK, Engelman DM. pH-(low)-insertion-peptide (pHLIP) translocation of membrane impermeable phalloidin toxin inhibits cancer cell proliferation. Proc Natl Acad Sci. 2010;107(47):20246–50. https://doi.org/10.1073/PNAS.1014403107

Ash WL, Stockner T, MacCallum JL, Tieleman DP. Computer modeling of polyleucine-based coiled coil dimers in a realistic membrane environment: insight into helix-helix interactions in membrane proteins. Biochemistry. 2004;43(28):9050–60. https://doi.org/10.1021/BI0494572

Avci FG, Akbulut BS, Ozkirimli E. Membrane active peptides and their biophysical characterization. Biomolecules. 2018;8(3):77. https://doi.org/10.3390/BIOM8030077

Batta G, Kárpáti L, Henrique GF, Tóth G, Tarapcsák S, Kovacs T, et al. Statin-boosted cellular uptake and endosomal escape of penetratin due to reduced membrane dipole potential. Br J Pharmacol. 2021;178(18):3667–81. https://doi.org/10.1111/bph.15509

Bechara C, Sagan S. Cell-penetrating peptides: 20 years later, where do we stand? FEBS Lett. 2013;587(12):1693–702. https://doi.org/10.1016/J.FEBSLET.2013.04.031

Bekker H, Berendsen H, Dijkstra E, Achterop S, VonDrumen R, VanDerSpoel D, et al. Gromacs: a parallel computer for molecular dynamics simulations. Physics Computing'92, pp. 252–256. 1993.

Bennett WFD, Sapay N, Tieleman DP. Atomistic simulations of pore formation and closure in lipid bilayers. Biophys J. 2014;106(1):210–9. https://doi.org/10.1016/J.BPJ.2013.11.4486/ASSET/B011580D-1A7B-4995-A11C-5EF27F0EF68E/MAIN.ASSETS/GR5.JPG

Berendsen HJC, van der Spoel D, van Drunen R. GROMACS: a message-passing parallel molecular dynamics implementation. Comput Phys Commun. 1995;91(1–3):43–56. https://doi.org/10.1016/0010-4655(95)00042-E

Bertrand J-R, Malvy C, Auguste T, Tóth GK, Kiss-Ivánkovits O, Illyés E, et al. Synthesis and studies on cell-penetrating peptides. Bioconjug Chem. 2009;20(7):1307–14. https://doi.org/10.1021/bc900005j

Catalina-Hernandez E, Aguilella-Arzo M, Peralvarez-Marin A, Lopez-Martin M. Computational insights into membrane disruption by cell-penetrating peptides. J Chem Inf Model. 2025;65(3):1549–59. https://doi.org/10.1021/ACS.JCIM.4C01940

Catalina-Hernandez E, Lopez-Martin M, Aguilella-Arzo M, Peralvarez-Marin A. Membrane disruption potential of endogenous opioid neuropeptide dynorphin a and related clinical variants. Int J Biol Macromol. 2025;316:144567. https://doi.org/10.1016/j.ijbiomac.2025.144567

Catalina-Hernandez E, Peralvarez-Marin A. Advances in molecular dynamics approaches for investigating cell-penetrating peptides. Biophys Rev. 2026;1–22. https://doi.org/10.1007/s12551-026-01409-y

Choe S. Free energy analyses of cell-penetrating peptides using the weighted ensemble method. Membranes. 2021;11(12):974. https://doi.org/10.3390/membranes11120974

Choe S. Translocation of a single Arg9 peptide across a DOPC/-DOPG(4:1) model membrane using the weighted ensemble method. Scientific Reports. 2023;13(1):1–9. https://doi.org/10.1038/s41598-023-28493-4

Copolovici DM, Langel K, Eriste E, Langel Ü. Cell-penetrating peptides: design, synthesis, and applications. ACS Nano. 2014;8(3):1972–94. https://doi.org/10.1021/nn4057269

Cruz J, Mihailescu M, Wiedman G, Herman K, Searson PC, Wimley WC, et al. A membrane-translocating peptide penetrates into bilayers without significant bilayer perturbations. Biophys J. 2013;104(11):2419–28. https://doi.org/10.1016/j.bpj.2013.04.043

Daggett V, Levitt M. Molecular dynamics simulations of helix denaturation. J Mol Biol. 1992;223(4):1121–38. https://doi.org/10.1016/0022-2836(92)90264-K

De Oliveira ECL, Da Costa KS, Taube PS, Lima AH, Junior CDSDS. Biological membrane-penetrating peptides: computational prediction and applications. Front Cell Infect Microbiol. 2022;12:838259. https://doi.org/10.3389/fcimb.2022.838259

Delemotte L, Tarek M. Molecular dynamics simulations of lipid membrane electroporation. J Membr Biol. 2012;245(9):531–43. https://doi.org/10.1007/s00232-012-9434-6

Derossi D, Calvet S, Trembleau A, Brunissen A, Chassaing G, Prochiantz A. Cell internalization of the third helix of the antennapedia homeodomain is receptor-independent *. J Biol Chem. 1996;271(30):18188–93. https://doi.org/10.1074/jbc.271.30.18188

Duchardt F, Fotin-Mleczek M, Schwarz H, Fischer R, Brock R. A comprehensive model for the cellular uptake of cationic cell-penetrating peptides. Traffic. 2007;8(7):848–66. https://doi.org/10.1111/J.1600-0854.2007.00572.X

Eiríksdóttir E, Konate K, Langel Ü, Divita G, Deshayes S. Secondary structure of cell-penetrating peptides controls membrane interaction and insertion. Biochim Biophys Acta. 2010;1798(6):1119–28. https://doi.org/10.1016/J.BBAMEM.2010.03.005

Endoh T, Ohtsuki T. Cellular siRNA delivery using cell-penetrating peptides modified for endosomal escape. Adv Drug Deliv Rev. 2009;61(9):704–9. https://doi.org/10.1016/J.ADDR.2009.04.005

Fanghänel S, Wadhwani P, Strandberg E, Verdurmen WPR, Bürck J, Ehni S, et al. Structure analysis and conformational transitions of the cell penetrating peptide Transportan 10 in the membrane-bound state. PLoS One. 2014;9(6):e99653. https://doi.org/10.1371/JOURNAL.PONE.0099653

Fathi N, Hojaji A, Bolhassani A, Agi E. Antitumor effects of HPV E7 and L1-E7 multiepitope DNA constructs delivered by synthetic and arginine-rich cell penetrating peptides. Int J Pept Res Ther. 2025;31(2):1–10. https://doi.org/10.1007/S10989-024-10679-7

Ferreira TM, Coreta-Gomes F, Samuli Ollila OH, Moreno MJ, Vaz WLC, Topgaard D. Cholesterol and POPC segmental order parameters in lipid membranes: solid state 1H-13C NMR and MD simulation studies. Phys Chem Chem Phys. 2013;15(6):1976–89. https://doi.org/10.1039/c2cp42738a

Fiedler S, Broecker J, Keller S. Protein folding in membranes. Cell Mol Life Sci. 2010;67(11):1779–98. https://doi.org/10.1007/S00018-010-0259-0

Fischli W, Goldstein A, Hunkapiller MW, Hood LE. Two "big" dynorphins from porcine pituitary. Life Sci. 1982;31(16–17):1769–72. https://doi.org/10.1016/0024-3205(82)90206-5

Frishman D, Argos P. Knowledge-based protein secondary structure assignment. Proteins. 1995;23(4):566–79. https://doi.org/10.1002/PROT.340230412

Futaki S, Suzuki T, Ohashi W, Yagami T, Tanaka S, Ueda K, et al. Arginine-rich peptides: an abundant source of membrane-permeable peptides having potential as carriers for intracellular protein delivery. J Biol Chem. 2001;276(8):5836–40. https://doi.org/10.1074/jbc.M007540200

Gestin M, Dowaidar M, Langel Ü. Uptake mechanism of cell-penetrating peptides. In: Sunna A, Care A, Bergquist PL, editors. Peptides and peptide-based biomaterials and their biomedical applications. Volume 1030. Cham: Springer International Publishing; 2017. p. 255–64. https://doi.org/10.1007/978-3-319-66095-0_11

Gowers R, Linke M, Barnoud J, Reddy T, Melo M, Seyler S, et al. MDAnalysis: a python package for the rapid analysis of molecular dynamics simulations. Python in Science Conference, 98–105. 2016 https://doi.org/10.25080/Majora-629e541a-00e

Gurtovenko AA, Vattulainen I. Pore formation coupled to ion transport through lipid membranes as induced by transmembrane ionic charge imbalance: atomistic molecular dynamics study. J Am Chem Soc. 2005;127(50):17570–1. https://doi.org/10.1021/ja053129n

Hasan M, Moghal MMR, Saha SK, Yamazaki M. The role of membrane tension in the action of antimicrobial peptides and cell-penetrating peptides in biomembranes. Biophys Rev. 2019;11(3):431–48. https://doi.org/10.1007/s12551-019-00542-1

He X, Lin M, Sha B, Feng S, Shi X, Qu Z, et al. Coarse-grained molecular dynamics studies of the translocation mechanism of polyarginines across asymmetric membrane under tension. Sci Rep. 2015;5:12808. https://doi.org/10.1038/SREP12808

Herce HD, Garcia AE. Molecular dynamics simulations suggest a mechanism for translocation of the HIV-1 TAT peptide across lipid membranes. Proc Natl Acad Sci. 2007;104(52):20805–10. https://doi.org/10.1073/pnas.0706574105

Hess B, Kutzner C, Van Der Spoel D, Lindahl E. GROMACS 4: algorithms for highly efficient, load-balanced, and scalable molecular

simulation. J Chem Theory Comput. 2008;4(3):435–47. https://doi.org/10.1021/CT700301Q
Hirose H, Takeuchi T, Osakada H, Pujals S, Katayama S, Nakase I, et al. Transient focal membrane deformation induced by arginine-rich peptides leads to their direct penetration into cells. Mol Ther. 2012;20(5):984–93. https://doi.org/10.1038/MT.2011.313
Hu Y, Liu X, Sinha SK, Patel S. Translocation thermodynamics of linear and cyclic nonaarginine into model dppc bilayer via coarse-grained molecular dynamics simulation: implications of pore formation and nonadditivity. J Phys Chem B. 2014;118(10):2670–82. https://doi.org/10.1021/jp412600e
Huang K, García AE. Free energy of translocating an arginine-rich cell-penetrating peptide across a lipid bilayer suggests pore formation. Biophys J. 2013;104(2):412–20. https://doi.org/10.1016/j.bpj.2012.10.027
Humphrey W, Dalke A, Schulten K. VMD: visual molecular dynamics. J Mol Graph. 1996;14(1):33–8. https://doi.org/10.1016/0263-7855(96)00018-5
Hunt JF, Rath P, Rothschild KJ, Engelman DM. Spontaneous, pH-dependent membrane insertion of a Transbilayer α-helix†. Biochemistry. 1997;36(49):15177–92. https://doi.org/10.1021/BI970147B
Hunter JD. Matplotlib: a 2D graphics environment. Comput Sci Eng. 2007;9(3):90–5. https://doi.org/10.1109/MCSE.2007.55
Illya G, Deserno M. Coarse-grained simulation studies of peptide-induced pore formation. Biophys J. 2008;95(9):4163–73. https://doi.org/10.1529/biophysj.108.131300
Ingólfsson HI, Carpenter TS, Bhatia H, Bremer PT, Marrink SJ, Lightstone FC. Computational Lipidomics of the neuronal plasma membrane. Biophys J. 2017;113(10):2271–80. https://doi.org/10.1016/j.bpj.2017.10.017
Irudayam SJ, Berkowitz ML. Binding and reorientation of melittin in a POPC bilayer: computer simulations. Biochim Biophys Acta. 2012;1818(12):2975–81. https://doi.org/10.1016/j.bbamem.2012.07.026
Islam MZ, Ariyama H, Alam JM, Yamazaki M. Entry of cell-penetrating peptide transportan 10 into a single vesicle by translocating across lipid membrane and its induced pores. Biochemistry. 2014;53(2):386–96. https://doi.org/10.1021/BI401406P
Islam MZ, Sharmin S, Levadnyy V, Alam Shibly SU, Yamazaki M. Effects of mechanical properties of lipid bilayers on the entry of cell-penetrating peptides into single vesicles. Langmuir. 2017;33(9):2433–43. https://doi.org/10.1021/acs.langmuir.6b03111
Iwasaki T, Tokuda Y, Kotake A, Okada H, Takeda S, Kawano T, et al. Cellular uptake and in vivo distribution of polyhistidine peptides. J Control Release. 2015;210:115–24. https://doi.org/10.1016/j.jconrel.2015.05.268
Jo S, Kim T, Iyer VG, Im W. CHARMM-GUI: a web-based graphical user interface for CHARMM. J Comput Chem. 2008;29(11):1859–65. https://doi.org/10.1002/jcc.20945
Jumper J, Evans R, Pritzel A, Green T, Figurnov M, Ronneberger O, et al. Highly accurate protein structure prediction with AlphaFold. Nature. 2021;596(7873):583–9. https://doi.org/10.1038/s41586-021-03819-2
Klimpel A, Lützenburg T, Neundorf I. Recent advances of anti-cancer therapies including the use of cell-penetrating peptides. Curr Opin Pharmacol. 2019;47:8–13. https://doi.org/10.1016/J.COPH.2019.01.003
Kluyver T, Ragan-Kelley B, Pérez F, Granger B, Bussonnier M, Frederic J, et al. Jupyter notebooks: a publishing format for reproducible computational workflows. In: Loizides F, Scmidt B, editors. 20th international conference on electronic publishing (01/01/16). The Netherlands: IOS Press; 2016. p. 87–90. https://doi.org/10.3233/978-1-61499-649-1-87
Kristensen M, Birch D, Nielsen HM. Applications and challenges for use of cell-penetrating peptides as delivery vectors for peptide and protein cargos. Int J Mol Sci. 2016;17(2):185. https://doi.org/10.3390/IJMS17020185
Kutzner C, Grubmüller H, De Groot BL, Zachariae U. Computational electrophysiology: the molecular dynamics of Ion Channel permeation and selectivity in atomistic detail. Biophys J. 2011;101(4):809–17. https://doi.org/10.1016/J.BPJ.2011.06.010
Kutzner C, Köpfer DA, Machtens JP, De Groot BL, Song C, Zachariae U. Insights into the function of ion channels by computational electrophysiology simulations. Biochim Biophys Acta. 2016;1858(7):1741–52. https://doi.org/10.1016/J.BBAMEM.2016.02.006
Kyte J, Doolittle RF. A simple method for displaying the hydropathic character of a protein. J Mol Biol. 1982;157(1):105–32. https://doi.org/10.1016/0022-2836(82)90515-0
Langel Ü. Cell-translocation mechanisms of CPPs. CPP, Cell-Penetrating Peptides, pp. 359–394. 2019 https://doi.org/10.1007/978-981-13-8747-0_10
Lee J, Cheng X, Swails JM, Yeom MS, Eastman PK, Lemkul JA, et al. CHARMM-GUI input generator for NAMD, GROMACS, AMBER, OpenMM, and CHARMM/OpenMM simulations using the CHARMM36 additive force field. J Chem Theory Comput. 2016;12(1):405–13. https://doi.org/10.1021/acs.jctc.5b00935
Lee J-H, Yang S-B, Park SJ, Kweon S, Ma G, Seo M, et al. Cell-penetrating peptide like anti-programmed cell death-ligand 1 peptide conjugate-based self-assembled nanoparticles for immunogenic photodynamic therapy. ACS Nano. 2025;19:2870–89. https://doi.org/10.1021/ACSNANO.4C16128
Lee MT, Chen FY, Huang HW. Energetics of pore formation induced by membrane active peptides. Biochemistry. 2004;43(12):3590–9. https://doi.org/10.1021/bi036153r
Lee M-T, Hung W-C, Chen F-Y, Huang HW. Many-body effect of antimicrobial peptides: on the correlation between Lipid's spontaneous curvature and pore formation. Biophys J. 2005;89(6):4006–16. https://doi.org/10.1529/biophysj.105.068080
Lee MT, Sun TL, Hung WC, Huang HW. Process of inducing pores in membranes by melittin. Proc Natl Acad Sci U S A. 2013;110(35):14243–8. https://doi.org/10.1073/pnas.1307010110
Leontiadou H, Mark AE, Marrink SJ. Molecular dynamics simulations of hydrophilic pores in lipid bilayers. Biophys J. 2004;86(4):2156–64. https://doi.org/10.1016/S0006-3495(04)74275-7
Leontiadou H, Mark AE, Marrink SJ. Antimicrobial peptides in action. J Am Chem Soc. 2006;128(37):12156–61. https://doi.org/10.1021/ja062927q
Levine ZA, Vernier PT. Life cycle of an electropore: field-dependent and field-independent steps in pore creation and annihilation. J Membr Biol. 2010;236(1):27–36. https://doi.org/10.1007/s00232-010-9277-y
Li T, Bourgeois J-P, Celli S, Glacial F, Le Sourd A-M, Mecheri S, et al. Cell-penetrating anti-GFAP VHH and corresponding fluorescent fusion protein VHH-GFP spontaneously cross the blood-brain barrier and specifically recognize astrocytes: application to brain imaging. FASEB J. 2012;26(10):3969–79. https://doi.org/10.1096/fj.11-201384
Lin YZ, Yao SY, Veach RA, Torgerson TR, Hawiger J. Inhibition of nuclear translocation of transcription factor NF-kappa B by a synthetic peptide containing a cell membrane-permeable motif and nuclear localization sequence. J Biol Chem. 1995;270(24):14255–8. https://doi.org/10.1074/jbc.270.24.14255
Lindahl E, Hess B, van der Spoel D. GROMACS 3.0: a package for molecular simulation and trajectory analysis. J Mol Model. 2001;7(8):306–17. https://doi.org/10.1007/S008940100045
Lindgren M, Hällbrink M, Prochiantz A, Langel Ü, Lindgren M, Hällbrink M, et al. Cell-penetrating peptides. Trends Pharmacol Sci. 2000;21(3):99–103. https://doi.org/10.1016/S0165-6147(00)01447-4
Liu BR, der Lin M, Chiang HJ, Lee HJ. Arginine-rich cell-penetrating peptides deliver gene into living human cells. Gene. 2012;505(1):37–45. https://doi.org/10.1016/j.gene.2012.05.053
Lopez CF, Nielsen SO, Srinivas G, DeGrado WF, Klein ML. Probing membrane insertion activity of antimicrobial polymers via

coarse-grain molecular dynamics. J Chem Theory Comput. 2006;2(3):649–55. https://doi.org/10.1021/ct050298p

MacCallum JL, Drew Bennett WF, Peter Tieleman D. Distribution of amino acids in a lipid bilayer from computer simulations. Biophys J. 2008;94(9):3393. https://doi.org/10.1529/BIOPHYSJ.107.112805

Madani F, Perálvarez-Marín A, Gräslund A. Liposome model systems to study the endosomal escape of cell-penetrating peptides: transport across phospholipid membranes induced by a proton gradient. J Drug Deliv. 2011;2011(1):897592. https://doi.org/10.1155/2011/897592

Magzoub M. Combating proteins with proteins: engineering cell-penetrating peptide antagonists of amyloid-β aggregation and associated neurotoxicity. DNA Cell Biol. 2020;39(6):920–5. https://doi.org/10.1089/dna.2020.5604

Magzoub M, Eriksson LEG, Gräslund A. Conformational states of the cell-penetrating peptide penetratin when interacting with phospholipid vesicles: effects of surface charge and peptide concentration. Biochim Biophys Acta. 2002;1563(1–2):53–63. https://doi.org/10.1016/S0005-2736(02)00373-5

Magzoub M, Kilk K, Eriksson LEG, Langel Ü, Gräslund A. Interaction and structure induction of cell-penetrating peptides in the presence of phospholipid vesicles. Biochim Biophys Acta. 2001;1512(1):77–89. https://doi.org/10.1016/S0005-2736(01)00304-2

Magzoub M, Pramanik A, Gräslund A. Modeling the endosomal escape of cell-penetrating peptides: transmembrane pH gradient driven translocation across phospholipid bilayers. Biochemistry. 2005;44(45):14890–7. https://doi.org/10.1021/BI051356W/ASSET/IMAGES/MEDIUM/BI051356WN00001.GIF

Maragliano L, Vanden-Eijnden E. A temperature accelerated method for sampling free energy and determining reaction pathways in rare events simulations. Chem Phys Lett. 2006;426(1–3):168–75. https://doi.org/10.1016/J.CPLETT.2006.05.062

Marks JR, Placone J, Hristova K, Wimley WC. Spontaneous membrane-translocating peptides by orthogonal high-throughput screening. J Am Chem Soc. 2011;133(23):8995–9004. https://doi.org/10.1021/JA2017416

Matsuzaki K, Yoneyama S, Murase O, Miyajima K. Transbilayer transport of ions and lipids coupled with Mastoparan X translocation. Biochemistry. 1996;35(25):8450–6. https://doi.org/10.1021/bi960342a

Michaud-Agrawal N, Denning EJ, Woolf TB, Beckstein O. MDAnalysis: a toolkit for the analysis of molecular dynamics simulations. J Comput Chem. 2011;32(10):2319–27. https://doi.org/10.1002/JCC.21787

Milletti F. Cell-penetrating peptides: classes, origin, and current landscape. Drug Discov Today. 2012;17(15–16):850–60. https://doi.org/10.1016/j.drudis.2012.03.002

Mirdita M, Schütze K, Moriwaki Y, Heo L, Ovchinnikov S, Steinegger M. ColabFold: making protein folding accessible to all. Nat Methods. 2022;19(6):679–82. https://doi.org/10.1038/s41592-022-01488-1

Mo RH, Zaro JL, Shen WC. Comparison of cationic and amphipathic cell penetrating peptides for siRNA delivery and efficacy. Mol Pharm. 2011;9(2):299–309. https://doi.org/10.1021/mp200481g

Moghal MR, Islam Z, Hossain F, Saha SK, Yamazaki M. Role of membrane potential on entry of cell-penetrating peptide Transportan 10 into single vesicles. Biophys J. 2020;118:57–69. https://doi.org/10.1016/j.bpj.2019.11.012

Muñoz-Gacitúa D, Guzman F, Weiss-López B. Insights into the equilibrium structure and translocation mechanism of TP1, a spontaneous membrane-translocating peptide. Sci Rep. 2022;12(1):1–10. https://doi.org/10.1038/s41598-022-23631-w

Nguyen MHL, DiPasquale M, Rickeard BW, Doktorova M, Heberle FA, Scott HL, et al. Peptide-induced lipid Flip-flop in asymmetric liposomes measured by small angle neutron scattering. Langmuir. 2019;35(36):11735–44. https://doi.org/10.1021/ACS.LANGMUIR.9B01625

Nymeyer H, Woolf TB, Garcia AE. Folding is not required for bilayer insertion: replica exchange simulations of an α-helical peptide with an explicit lipid bilayer. Proteins Struct Funct Bioinform. 2005;59(4):783–90. https://doi.org/10.1002/prot.20460

Oba M, Nakajima S, Misao K, Yokoo H, Tanaka M. Effect of helicity and hydrophobicity on cell-penetrating ability of arginine-rich peptides. Bioorg Med Chem. 2023;91:117409. https://doi.org/10.1016/J.BMC.2023.117409

Ouyang J, Sheng Y, Wang W. Recent advances of studies on cell-penetrating peptides based on molecular dynamics simulations. Cells. 2022;11(24):4016. https://doi.org/10.3390/cells11244016

Páll S, Abraham MJ, Kutzner C, Hess B, Lindahl E. Tackling exascale software challenges in molecular dynamics simulations with GROMACS. Lecture Notes in Computer Science (Including Subseries Lecture Notes in Artificial Intelligence and Lecture Notes in Bioinformatics). 2015;8759:3–27. https://doi.org/10.1007/978-3-319-15976-8_1

Park S, Kim J, Oh SS, Choi SQ. Arginine-rich cell-penetrating peptides induce lipid rearrangements for their active translocation across laterally heterogeneous membranes. Adv Sci. 2024;11:e2404563. https://doi.org/10.1002/advs.202404563

Piggot TJ, Allison JR, Sessions RB, Essex JW. On the calculation of acyl chain order parameters from lipid simulations. J Chem Theory Comput. 2017;13(11):5683–96. https://doi.org/10.1021/acs.jctc.7b00643

Pouny Y, Rapaport D, Mor A, Nicolas P, Shai Y. Interaction of antimicrobial dermaseptin and its fluorescently labeled analogs with phospholipid membranes. Biochemistry. 1992;31(49):12416–23. https://doi.org/10.1021/bi00164a017

Pronk S, Páll S, Schulz R, Larsson P, Bjelkmar P, Apostolov R, et al. GROMACS 4.5: a high-throughput and highly parallel open source molecular simulation toolkit. Bioinformatics. 2013;29(7):845–54. https://doi.org/10.1093/BIOINFORMATICS/BTT055

Rashid MMO, Moghal MMR, Billah MM, Hasan M, Yamazaki M. Effect of membrane potential on pore formation by the antimicrobial peptide magainin 2 in lipid bilayers. Biochim Biophys Acta. 2020;1862(10):183381. https://doi.org/10.1016/j.bbamem.2020.183381

Reid LM, Verma CS, Essex JW. The role of molecular simulations in understanding the mechanisms of cell-penetrating peptides. Drug Discov Today. 2019;24(9):1821–35. https://doi.org/10.1016/j.drudis.2019.06.013

Repáková J, Holopainen JM, Morrow MR, McDonald MC, Čapková P, Vattulainen I. Influence of DPH on the structure and dynamics of a DPPC bilayer. Biophys J. 2005;88(5):3398–410. https://doi.org/10.1529/biophysj.104.055533

Richard JP, Melikov K, Brooks H, Prevot P, Lebleu B, Chernomordik LV. Cellular uptake of unconjugated TAT peptide involves clathrin-dependent endocytosis and heparan sulfate receptors. J Biol Chem. 2005;280(15):15300–6. https://doi.org/10.1074/jbc.M401604200

Ruseska I, Zimmer A. Internalization mechanisms of cell-penetrating peptides. Beilstein J Nanotechnol. 2020;2020:101–23. https://doi.org/10.3762/bjnano.11.10

Säälik P, Elmquist A, Hansen M, Padari K, Saar K, Viht K, et al. Protein cargo delivery properties of cell-penetrating peptides. A comparative study. Bioconjug Chem. 2004;15(6):1246–53. https://doi.org/10.1021/BC049938Y

Sahni A, Qian Z, Pei D. Cell-penetrating peptides escape the endosome by inducing vesicle budding and collapse. ACS Chem Biol. 2020;15(9):2485–92. https://doi.org/10.1021/ACSCHEMBIO.0C00478

Sahni A, Ritchey JL, Qian Z, Pei D. Cell-penetrating peptides translocate across the plasma membrane by inducing vesicle budding

and collapse. J Am Chem Soc. 2024;146(36):25371–82. https://doi.org/10.1021/JACS.4C10533
Sani MA, Separovic F. How membrane-active peptides get into lipid membranes. Acc Chem Res. 2016;49(6):1130–8. https://doi.org/10.1021/acs.accounts.6b00074
Sengupta D, Leontiadou H, Mark AE, Marrink SJ. Toroidal pores formed by antimicrobial peptides show significant disorder. Biochim Biophys Acta. 2008;1778(10):2308–17. https://doi.org/10.1016/J.BBAMEM.2008.06.007
Sharmin S, Islam MZ, Karal MAS, Alam Shibly SU, Dohra H, Yamazaki M. Effects of lipid composition on the entry of cell-penetrating peptide oligoarginine into single vesicles. Biochemistry. 2016;55(30):4154–65. https://doi.org/10.1021/acs.biochem.6b00189
Silva S, Almeida AJ, Vale N. Combination of cell-penetrating peptides with nanoparticles for therapeutic application: a review. Biomolecules. 2019;9(1):22. https://doi.org/10.3390/biom9010022
Smith AP, Lee NM. Pharmacology of dynorphin. Annu Rev Pharmacol Toxicol. 1988;28:123–40. https://doi.org/10.1146/annurev.pa.28.040188.001011
Song W, Corey RA, Ansell TB, Cassidy CK, Horrell MR, Duncan AL, et al. PyLipID: a python package for analysis of protein–lipid interactions from molecular dynamics simulations. J Chem Theory Comput. 2022;18(2):1188–201. https://doi.org/10.1021/acs.jctc.1c00708
Soomets U, Lindgren M, Gallet X, Hällbrink M, Elmquist A, Balaspiri L, et al. Deletion analogues of transportan. Biochim Biophys Acta. 2000;1467(1):165–76. https://doi.org/10.1016/S0005-2736(00)00216-9
Steiner V, Schzr M, B&men KO, Mutter M. Retention behaviour of a template-assembled synthetic protein and its amphiphilic building blocks on reversed-phase columns. J Chromatogr. 1991;586(1):43–50. https://doi.org/10.1016/0021-9673(91)80023-A
Sun D, Forsman J, Lund M, Woodward CE. Effect of arginine-rich cell penetrating peptides on membrane pore formation and life-times: a molecular simulation study. Phys Chem Chem Phys. 2014;16(38):20785–95. https://doi.org/10.1039/c4cp02211d
Sun D, Forsman J, Woodward CE. Atomistic molecular simulations suggest a kinetic model for membrane translocation by arginine-rich peptides. J Phys Chem B. 2015;119(45):14413–20. https://doi.org/10.1021/ACS.JPCB.5B08072
Tarek M. Membrane electroporation: a molecular dynamics simulation. Biophys J. 2005;88(6):4045–53. https://doi.org/10.1529/BIOPHYSJ.104.050617/ASSET/DD8E30C9-0279-4AE1-9B48-6C5AFE67C0A5/MAIN.ASSETS/GR5.JPG
Thi Hong Nguyen M. Biologically relevant ions and peptides in aqueous solutions and at model. 2024.
Thi Hong Nguyen M, Vazdar M. Molecular dynamics simulations unveil the aggregation patterns and salting out of polyarginines at zwitterionic POPC bilayers in solutions of various ionic strengths. Comput Struct Biotechnol J. 2024;23:3897–905. https://doi.org/10.1016/j.csbj.2024.11.004
Thorén PEG, Persson D, Esbjörner EK, Goksör M, Lincoln P, Nordén B. Membrane binding and translocation of cell-penetrating peptides†. Biochemistry. 2004;43(12):3471–89. https://doi.org/10.1021/BI0360049
Thorén PEG, Persson D, Isakson P, Goksör M, Önfelt A, Nordén B. Uptake of analogs of penetratin, tat(48–60) and oligoarginine in live cells. Biochem Biophys Res Commun. 2003;307(1):100–7. https://doi.org/10.1016/S0006-291X(03)01135-5
Tieleman DP. The molecular basis of electroporation. BMC Biochem. 2004;5(1):1–12. https://doi.org/10.1186/1471-2091-5-10
Tieleman DP, Leontiadou H, Mark AE, Marrink SJ. Simulation of pore formation in lipid bilayers by mechanical stress and electric fields. J Am Chem Soc. 2003;125(21):6382–3. https://doi.org/10.1021/JA029504I
Tieleman DP, Marrink S-J. Lipids out of Equilibrium: Energetics of Desorption and Pore Mediated Flip-Flop. J Am Chem Soc. 2006;128:12462–7. https://doi.org/10.1021/ja0624321
Torrie GM, Valleau JP. Nonphysical sampling distributions in Monte Carlo free-energy estimation: umbrella sampling. J Comput Phys. 1977;23(2):187–99. https://doi.org/10.1016/0021-9991(77)90121-8
Trofimenko E, Grasso G, Heulot M, Chevalier N, Deriu MA, Dubuis G, et al. Genetic, cellular, and structural characterization of the membrane potential-dependent cell-penetrating peptide translocation pore. Elife. 2021;10:e69832. https://doi.org/10.7554/ELIFE.69832
Van Der Spoel D, Lindahl E, Hess B, Groenhof G, Mark AE, Berendsen HJC. GROMACS: fast, flexible, and free. J Comput Chem. 2005;26(16):1701–18. https://doi.org/10.1002/JCC.20291
Veldhoen S, Laufer SD, Trampe A, Restle T. Cellular delivery of small interfering RNA by a non-covalently attached cell-penetrating peptide: quantitative analysis of uptake and biological effect. Nucleic Acids Res. 2006;34(22):6561–73. https://doi.org/10.1093/NAR/GKL941
Vernier PT, Ziegler MJ, Sun Y, Chang WV, Gundersen MA, Tieleman DP. Nanopore formation and phosphatidylserine externalization in a phospholipid bilayer at high transmembrane potential. J Am Chem Soc. 2006;128(19):6288–9. https://doi.org/10.1021/ja0588306
Virtanen P, Gommers R, Oliphant TE, Haberland M, Reddy T, Cournapeau D, et al. SciPy 1.0: fundamental algorithms for scientific computing in python. Nat Methods. 2020;17(3):261–72. https://doi.org/10.1038/s41592-019-0686-2
Wang Y, Gallagher E, Jorgensen C, Troendle EP, Hu D, Searson PC, et al. An experimentally validated approach to calculate the blood-brain barrier permeability of small molecules. Sci Rep. 2019;9:1–11. https://doi.org/10.1038/s41598-019-42272-0
Weaver JC, Chizmadzhev YA. Theory of electroporation: a review. Bioelectrochem Bioenerg. 1996;41(2):135–60. https://doi.org/10.1016/S0302-4598(96)05062-3
Weng J, Wang A, Zhang D, Liao C, Li G. A double bilayer to study the nonequilibrium environmental response of GIRK2 in complex states. Phys Chem Chem Phys. 2021;23:15784–95. https://doi.org/10.1039/d1cp01785c
Whitley P, Grau B, Gumbart JC, Martínez-Gil L, Mingarro I. Folding and insertion of transmembrane helices at the ER. Int J Mol Sci. 2021;22(23):12778. https://doi.org/10.3390/IJMS222312778
Wolf J, Aisenbrey C, Harmouche N, Raya J, Bertani P, Voievoda N, et al. pH-dependent membrane interactions of the histidine-rich cell-penetrating peptide LAH4-L1. Biophys J. 2017;113(6):1290–300. https://doi.org/10.1016/j.bpj.2017.06.053
Wu EL, Cheng X, Jo S, Rui H, Song KC, Dávila-Contreras EM, et al. CHARMM-GUI membrane builder toward realistic biological membrane simulations. J Comput Chem. 2014;35(27):1997–2004. https://doi.org/10.1002/jcc.23702
Wu H, Zhuang Q, Xu J, Xu L, Zhao Y, Wang C, et al. Cell-penetrating peptide enhanced antigen presentation for cancer immunotherapy. Bioconjug Chem. 2019;30(8):2115–26. https://doi.org/10.1021/ACS.BIOCONJCHEM.9B00245
Yandek LE, Pokorny A, Florén A, Knoelke K, Langel Ü, Almeida PFF. Mechanism of the cell-penetrating peptide Transportan 10 permeation of lipid bilayers. Biophys J. 2007;92(7):2434–44. https://doi.org/10.1529/BIOPHYSJ.106.100198
Yang L, Harroun TA, Weiss TM, Ding L, Huang HW. Barrel-stave model or toroidal model? A case study on melittin pores. Biophys J. 2001;81(3):1475–85. https://doi.org/10.1016/S0006-3495(01)75802-X
Yesylevskyy S, Marrink SJ, Mark AE. Alternative mechanisms for the interaction of the cell-penetrating peptides penetratin and

the TAT peptide with lipid bilayers. Biophys J. 2009;97(1):40–9. https://doi.org/10.1016/j.bpj.2009.03.059

Zakany F, Mándity IM, Varga Z, Panyi G, Nagy P, Kovacs T. Effect of the lipid landscape on the efficacy of cell-penetrating peptides. Cells. 2023;12(13):1700. https://doi.org/10.3390/cells12131700

SUPPORTING INFORMATION

Additional supporting information can be found online in the Supporting Information section at the end of this article.

How to cite this article: Catalina-Hernandez E, Aguilella-Arzo M, Lopez-Martin M, Peralvarez-Marin A. Understanding cell-penetrating peptide mechanisms using computational electrophysiology simulations. Protein Science. 2026;35(4):e70536. https://doi.org/10.1002/pro.70536